The role of interfacial tension in the size-dependent phase separation of atmospheric aerosol particles

Ryan Schmedding[1] and Andreas Zuend[1]

[1]Department of Atmospheric and Oceanic Sciences, McGill University, Montreal, Quebec, Canada
Correspondence: Andreas Zuend (andreas.zuend@mcgill.ca)

Abstract. Atmospheric aerosol particles span orders of magnitude in size. In ultrafine particles, the energetic contributions of surfaces and interfaces to the Gibbs energy become significant and increase in importance as particle diameter decreases. For these particles, the thermodynamic equilibrium state depends on size, composition, and temperature. Various aerosol systems have been observed to undergo liquid–liquid phase separation (LLPS), impacting equilibrium gas–particle partitioning,
5 modifying physicochemical properties of the particle phases, and influencing cloud droplet activation. Numerous laboratory experiments have characterized the onset relative humidity of LLPS in larger aerosol particles and macroscopic bulk systems. However, in sufficiently small particles, the interfacial tension between two liquid phases constitutes an energetic barrier that may prevent the formation of an additional liquid phase. Determining said small-size limit is a key question.

We introduce a predictive droplet model based on the Aerosol Inorganic–Organic Mixtures Functional groups Activity
10 Coefficients model. This model enables size-dependent computations of surface and interfacial tension effects on bulk–surface partitioning within phase-separated and single-phase particles. We evaluate four approaches for computing interfacial tension in multicomponent droplets, including a new method introduced in this work. Of the approaches tested, Antonov's rule best matches observed liquid–liquid interfacial tensions in highly immiscible mixtures, while a modified Butler equation fits well in more miscible systems. We find that two approaches substantially lower the onset relative humidity of LLPS for the studied
15 systems.

1 Introduction

Atmospheric aerosols and their interactions with clouds and radiation are a major source of uncertainty in global climate models (Intergovernmental Panel on Climate, 2014). The condensed particle phase component of an aerosol, henceforth referred to as aerosol particles or "aerosols" varies in composition regionally and over time (Jimenez et al., 2009). Organic com-
20 pounds contribute a substantial mass fraction to the total condensed material within ambient aerosols. Organic-rich particles can be emitted directly (primary organic aerosols) or formed from gas-phase reactions involving volatile organic compounds (VOCs). Aerosols which contain substantial amounts of secondary organic compounds are often referred to as secondary organic aerosols (SOA). For complete lists of abbreviations, symbols, and their meanings, please refer to Tables S1 and S2 in the supplementary information. SOA mixed with inorganic species such as dissolved aqueous electrolytes form the majority

25 of fine-mode aerosols in many regions of the world (Zhang et al., 2007). Therefore, understanding the properties of aerosol particles is important for better constraints on global air quality and climate models and related future climate projections.

The effects of a population of aerosol particles on weather and climate depend on the collective properties of the particles. Two properties which have been the focus of numerous studies are the number of condensed phases present in an aerosol particle and the morphology of the particle, whether said particle is of spherical or non-spherical shape, or consists of a com-

30 bination of smaller three-dimensional structures (Kucinski et al., 2019; Ohno et al., 2023). Liquid–liquid phase separation (LLPS) has been observed in numerous laboratory-generated and atmospheric aerosols, with many particles of varying compositions splitting into two distinct phases in contact with one another (Marcolli and Krieger, 2006; You et al., 2012; Ciobanu et al., 2009; Bertram et al., 2011; Freedman, 2017). More recently, the presence of three liquid phases within single aerosol particles has been observed in laboratory mimics of urban aerosols (Huang et al., 2021; Kucinski et al., 2019). The unique

35 composition of each liquid phase present in a particle determines a range of the physicochemical properties of those phases and/or a particle overall. These properties include the hygroscopicity and related equilibrium water content, the surface tension, viscosity, acidity, and ionic strength, all of which may vary as a function of environmental (thermodynamic) conditions and phase-specific composition Lilek and Zuend (2022); Gervasi et al. (2020); Schmedding and Zuend (2023); Kleinheins et al. (2023). Organic-rich phases may exhibit atmospherically relevant physical properties similar to that of an aqueous electrolyte-

40 containing phase or properties which are quite different than those of the aqueous ion-rich phase (Li et al., 2021; Chan et al., 2006). These properties may affect the growth and aging of aerosol particles by limiting the reactive uptake of species such as isoprene-derived epoxydiols, or N_2O_5 (Gaston et al., 2014; Schmedding et al., 2020). Aerosol–cloud interactions can also be affected by the presence of liquid–liquid phase separation in aerosol particles, especially so if LLPS persists to high relative humidities (RH) (Ovadnevaite et al., 2017; Malek et al., 2023). The reduction in droplet surface tension typically caused by an

45 enrichment of organics at the gas–particle surface and the coupled simultaneous modification to the bulk phase composition due to bulk–surface partitioning, have competing effects on the water vapor saturation ratio and minimum dry particle size necessary for cloud droplet activation. This can ultimately lead to a substantial shift in the critical saturation ratio and diameter necessary for the activation of aerosol particles into cloud droplets (Ruehl et al., 2016; Ovadnevaite et al., 2017; Davies et al., 2019; Schmedding and Zuend, 2023).

50 Beyond changes to the physicochemical properties of aerosol particles stemming from the formation of distinct condensed phases within a particle, the three-dimensional (3-D) morphology of a particle may be modified. Homogeneously mixed particles assume a spherical shape under equilibrium conditions due to the impact of surface tension. In the case of a phase-separated particle, deviations from sphericity are possible (Kwamena et al., 2010; Gorkowski et al., 2020). Some LLPS particles still form an overall spherical structure with an organic-rich shell (phase β) covering an inorganic-rich core (phase α). Other, more com-

55 plex structures are possible, such as a partially engulfed morphology, wherein the particle is no longer radially symmetric nor perfectly spherical. In a partially engulfed particle, phase β does not spread completely over phase α and leaves a portion of phase α exposed (Kwamena et al., 2010; Reid et al., 2011; Ciobanu et al., 2009; Song et al., 2012, 2013; Shiraiwa et al., 2013). Such particle geometries interact with radiation differently than their core–shell counterparts (Lang-Yona et al., 2010). It has also been observed that LLPS particles composed of 3-methylglutaric acid and ammonium sulfate, which have a core–shell

morphology at higher RH, form partially engulfed particles at lower RH (Lam et al., 2021). Should additional condensed phases be present beyond the simplest two-phase case, various combinations of spherical shells and partially engulfing phases are possible (Huang et al., 2021), leading to geometric structures which may be highly complex. Under equilibrium conditions, the sequence of these phases in terms of the innermost to outermost phase of the particle is determined by the configuration which minimizes the overall Gibbs energy of the particle. Usually, this results in arrangements that favor placing the phases with higher hypothetical gas–liquid surface tensions closer to the center of the particle, while those with lower surface tensions are closer to or at the gas–particle boundary.

Analogous to the surface between a gas phase and a condensed phase, the interface between two condensed phases, particularly two liquid phases, might experience a similar phenomenon with respect to the enrichment and depletion of different compounds (Hua et al., 2016). Note that hereafter in this article, "surface" refers to a gas–liquid phase boundary and "interface" refers to the boundary between two condensed (liquid) phases. There have been several attempts to quantify the relative contribution of the liquid–liquid (LL) interface between two condensed phases to the overall energy of a particle and whether bulk phase depletion plays a role at the LL interface. Until recently, it has been assumed that the energetic contributions from LL interfacial tension in typical aerosol particles are negligible for particles with diameters larger than approximately $100\,\mathrm{nm}$, for which the Kelvin effect is also relatively minor (Russell and Ming, 2002; Zuend et al., 2010). Despite this, recent studies have found that the contribution of a LL interface to the Gibbs energy of a particle may have a small but not insignificant effect on the RH at which the particle will undergo LLPS upon dehydration (Ohno et al., 2023).

In order to better understand the role of interfacial tension and its interaction with phase separation and particle morphologies, predictive models of interfacial tension and associated phase composition changes are necessary. Different approaches have been considered for the prediction of liquid–liquid interfacial tension; a brief overview is presented in the following, with additional theory and methods discussed in Sect. 2.

The simplest approximation for the interfacial tension between two phases α and β, $\sigma^{\alpha\beta}$, is by taking the absolute difference of the hypothetical gas–liquid surface tensions of the two phases (σ^{α} and σ^{β}) when each is considered in isolation,

$$\sigma^{\alpha\beta} = \left| \sigma^{\alpha} - \sigma^{\beta} \right|. \tag{1}$$

Equation (1) is known as Antonov's rule (Antonov, 1907). While Eq. (1) may be a good first-order approximation of the interfacial tension for some systems, it is an empirical estimation method and not thermodynamically rigorous (Makkonen and Kurkela, 2018; Winter, 1995). A distinct approach for determining the interfacial tension between two liquid phases was proposed by Girifalco and Good (1957):

$$\sigma^{\alpha\beta} = \sigma^{\alpha} + \sigma^{\beta} - 2\phi\sqrt{\sigma^{\alpha}\sigma^{\beta}}, \tag{2}$$

where ϕ is a system-dependent interaction/correction parameter. It has been shown that ϕ may be constrained by the following inequality:

$$\phi \geq \left(1 - \frac{\sigma^{\alpha\beta}}{\sigma^{\alpha}}\right)^{\frac{1}{2}}. \tag{3}$$

Note that in the case of a single well-mixed phase, where $\sigma^{\alpha\beta} = 0$, $\phi = 1$. In the limiting case where $\phi = \left(1 - \frac{\sigma^{\alpha\beta}}{\sigma^{\alpha}}\right)^{\frac{1}{2}}$, Eq. (2) reduces to Eq. (1). However, the utility of this equation for systems with more than two components, or with compounds that are soluble in both phases, remains an open question (Makkonen and Kurkela, 2018). Equation. (2) was further refined to

$$\sigma^{\alpha\beta} = \sigma^{\alpha} + \sigma^{\beta} - 2\left(\sigma^{\alpha,\text{disp}} \cdot \sigma^{\beta,\text{disp}}\right)^{\frac{1}{2}}, \tag{4}$$

where $\sigma^{\alpha,\text{disp}}$ and $\sigma^{\beta,\text{disp}}$ are the contributions from dispersion forces to the surface tensions of phases α and β, respectively (Fowkes, 1962, 1963). Of course, such a model relies on accurate constraints on the dispersive and non-dispersive contributions to the surface energies per unit area of both phases, thus limiting the utility of this approach.

As mentioned above, some atmospheric aerosol systems have been observed to undergo LLPS for particles with large diameters, yet particles of the same or similar composition may not undergo LLPS should their diameters be substantially smaller (Kucinski et al., 2019; Freedman, 2020; Ott and Freedman, 2020; Ohno et al., 2023). Indeed, it is thought that at sufficiently small diameters, the high surface area to volume ratios of atmospheric aerosol particles lead to a sufficient energetic barrier from the combined effects of surface and interfacial tensions that the formation of an additional phase is inhibited (Ohno et al., 2023; Freedman, 2020). It should be noted that the effect of aerosol composition, particularly the presence of different inorganic electrolytes, complicates size-dependent LLPS; for example, Ott and Freedman (2021) report that particles containing sodium cations are phase-separated down to smaller sizes than similar particles which contain ammonium cations.

To our knowledge, no predictive model exists that accounts for the coupled feedbacks of aerosol particle size and three-dimensional morphology on the conditions under which a particle will separate into two (or more) liquid phases or remain homogeneously mixed. As such, we present a thermodynamic framework for exploring and quantifying the size-dependent LLPS in aerosol particles.

2 Methods

2.1 Modeling interfacial tension between two liquid phases

In the case of a closed thermodynamic system with two or more liquid phases, the Gibbs energy at constant temperature and pressure can be expressed as follows:

$$G = \sum_{\phi} \sum_{j} \mu_j^{\phi} n_j^{\phi} + \sum_{\iota} \sigma^{\iota} A^{\iota} + \tau l. \tag{5}$$

Here, μ_j^ϕ and n_j^ϕ are the chemical potential and molar amount of species j in phase ϕ. σ^ι is the surface or interfacial tension at phase boundary ι and A^ι is the area of phase boundary ι. τ represents the energetic contribution of a 3-phase boundary line, sometimes referred to as the line tension, and l is the length of the 3-phase boundary line. Note that a 3-phase boundary line will only exist in a particle with a partially engulfed morphology or when particles are deposited on a substrate for analysis

120 in laboratory experiments. Furthermore, given that measured and predicted line energy contributions in complex systems are thought to be orders of magnitude lower than those from LL interface contributions, energetic contributions from the τl term is usually assumed to be negligible (Amirfazli and Neumann, 2004).

Schmedding and Zuend (2023) developed an approach for predicting the equilibrium surface tension of a single-liquid-phase droplet with a finite-depth Guggenheim interface of radial thickness δ^s. Their approach employed the Aerosol Inorganic

125 Mixtures Functional groups Activity Coefficients (AIOMFAC) model (Zuend et al., 2008, 2011; Yin et al., 2022) to calculate activity coefficients in the surface and bulk phases of an aerosol particle for application in the Butler equation:

$$\sigma_i = \sigma_i^\circ + \frac{RT}{\mathscr{A}_i} \ln\left(\frac{a_i^s}{a_i^b}\right). \tag{6}$$

Here, σ_i is the surface tension of the droplet as predicted by the right-hand-side expression based on component i, σ_i° is the surface tension of i in the pure-component case at the same pressure and temperature, R is the universal gas constant, T is

130 the temperature, $\mathscr{A}_i$ is the partial molar area of i, which depends on the surface phase geometry, a_i^s is the mole-fraction-based activity of i in the surface phase and a_i^b is the mole fraction-based (or molality-based, in the case of inorganic electrolytes) activity of i in the liquid bulk phase. a_i^b can be calculated as the product of the concentration of species i, either in mole fraction or molality as previously mentioned, and the activity coefficient, γ_i, at a given temperature on the associated composition scale. Under equilibrium conditions the surface tensions computed via Eq. (6) for all k components in solution must be equal, such

135 that

$$\sigma_1 = \sigma_2 = ... = \sigma_k. \tag{7}$$

While the structure of a gas–liquid interface may be best represented by a thin, yet finite-depth surface phase to account for bulk–surface partitioning, the structure of a LL interface may be more easily represented by a two-dimensional (2-D) dividing surface. The latter is the case since the absolute material and density gradients across LL interfaces are much smaller than across

140 a gas–liquid surface. Therefore, unlike the approach to bulk–surface partitioning described in Schmedding and Zuend (2023), there is no depletion from phase α nor phase β to the LL interface between them as the tightly coupled partitioning between phases α and β accounts for the depletion of either phase with respect to the LL interface. Note, however, that modifications to the equilibrium partitioning of components between the two liquid phases due to the presence of the interface can be accounted for. This 2-D LL interface treatment has the added benefit of simplifying the approach used to determine the interfacial tension

145 as the interplay between partitioning and non-ideal mixing may be greatly simplified in the liquid–liquid interface.

Returning to the approach of Schmedding and Zuend (2023), which utilized Eq. (6) to predict surface tension, we now extend the same approach to account for the boundary between two liquid phases. For a LL interface Eq. (6) must be modified, since the reference state surface tension values (σ_i°) are inherently different from those found at the gas–liquid surface. At a gas–liquid boundary, σ_i° is assumed to be surface tension of a droplet of pure component i. Analogously, for LL interfaces, σ_i° is

150 assumed to be the interfacial tension that exists between two molecular layers of pure component i. Because the compositions of the two layers of i are identical in the LL reference state case – a hypothetical interface – any molecule present at this reference LL interface would not experience an additional energetic penalty. Therefore, in the case of a LL interface,

$$\sigma_1^{\alpha\beta,\circ} = \sigma_2^{\alpha\beta,\circ} = ... = \sigma_k^{\alpha\beta,\circ} = 0. \tag{8}$$

Consequently, in the case of a LL interface, Eq. (6) simplifies to (Bahramian and Danesh, 2005, 2004):

155 $$\sigma_i^{\alpha\beta} = \frac{RT}{\mathscr{A}_i^{\alpha\beta}} \ln\left(\frac{a_i^{\alpha\beta}}{a_i^{\mathrm{b}}}\right). \tag{9}$$

Analogous to Eq. (7), the interfacial tension values determined via Eq. (9) for individual components must match at equilibrium, i.e.,

$$\sigma_1^{\alpha\beta} = \sigma_2^{\alpha\beta} = ... = \sigma_3^{\alpha\beta}. \tag{10}$$

An approach developed by Bahramian and Danesh (2004) utilized lattice theory and suggested that the activity coefficients

160 present in a LL interface ($\gamma^{\alpha\beta}$) can be approximated by the geometric mean of the activity coefficients in the liquid phases α and β on either side of the interface:

$$\gamma_i^{\alpha\beta} = \sqrt{\gamma_i^\alpha \gamma_i^\beta}. \tag{11}$$

However, they note that the choice of $\frac{1}{2}$ for the exponent in this case is determined by the configuration of molecules present in the interfacial region. This approach was also later expanded by Wang and Anderko (2013) to account for the effect of

165 electrolyte species in mixed organic–inorganic systems with good agreement to experimental data. Therefore, in this study, the geometric mean approach for activity coefficients was chosen as one option for multicomponent aerosol systems containing mixtures of water, organic species, and electrolytes.

If the assumption of Eq. (11) is used, and recalling that under equilibrium conditions $x_i^\alpha \gamma_i^\alpha = x_i^\beta \gamma_i^\beta$ and $\sum x_i^{\alpha\beta} = 1$, Eq. (9) can be rearranged to the following form (Bahramian and Danesh, 2004, 2005):

170 $$\sum_i \sqrt{x_i^\beta x_i^\alpha} \exp\left(\frac{\mathscr{A}_i^{\alpha\beta} \sigma^{\alpha\beta}}{RT}\right) = 1. \tag{12}$$

This leads to a single unknown variable, $\sigma^{\alpha\beta}$, which must be the same for all species such that the criteria given by Eq. (10) are satisfied. Thus, the interfacial tension value can be solved for numerically in a direct manner, rather than relying on a more complex bulk–interface partitioning algorithm (unlike the case for bulk–surface partitioning). It should be noted that the behavior of electrolyte species in solution may require more complex treatments of their impacts on interfacial tension (Wang and Anderko, 2013). However, many of these treatments rely on semi-empirical relationships fitted to experimental data, thus reducing their predictive power and flexibility. As such, in this approach we assume that electrolyte components (here as neutral cation–anion combinations) can be treated in the same manner as water and the organic components.

2.2 Alternative models of interfacial tension

In order to determine the importance of a rigorous treatment of interfacial energetic contributions in aerosol particles and the resulting geometric morphologies, we introduce the following approaches, allowing for a quantitative comparison (see Sect. 3). A first option is a model which allows for LLPS and bulk–surface partitioning, but assumes that the LL interface is a 2-D dividing surface with an energetic contribution of 0 (labeled as "no IFE" approach).

A more thorough treatment includes assuming a 2-D LL interface with the interfacial tension value estimated by the difference in (hypothetical) gas–liquid surface tensions of the organic phase and the aqueous phase (Eq. 1) (Antonov's rule). One caveat of this treatment is that it renders determining whether a particle is of core–shell or partially engulfed morphology impossible. This is because of a known inconsistency of Antonov's rule with the constraints imposed by the triangle inequality necessary for calculating the contact angles among the phases (Binyaminov et al., 2021). As a similar option, Eq. (2) can be employed as a semi-empirical representation of the LL interfacial tension. This Girifalco–Good equation can be tuned with a single, system-specific parameter ϕ to improve agreement with pertinent experimental data.

A final semi-empirical approach for the LL interfacial tension is based on a modified version of the approach of Bahramian (2024), who stated that $x_i^{\alpha\beta} \geq \sqrt{x_i^{\alpha} x_i^{\beta}}$. In this case, we treat the composition of the interfacial layer as the weighted average of the compositions of a monolayer of phase α and β on either side of the 2-D dividing plane such that

$$v_i^{\alpha\beta} = \left(v_i^{\alpha} v_i^{\beta} \right)^{\eta}. \tag{13}$$

Here, v_i is the effective volume fraction of i in phase α, phase β, or the two (mono)layers of α and β immediately adjacent to the interfacial dividing plane (the hypothetical interfacial bilayer). η is defined as the value that satisfies the criteria that $\sum \left(v_i^{\alpha} v_i^{\beta} \right)^{\eta} = 1$ and $\eta > 0$ in order to satisfy the criteria of (Bahramian, 2024). A reference energetic contribution value for this bilayer system can be estimated by

$$\sigma^{\alpha\beta,\circ} = \sum \left(v_i^{\alpha} v_i^{\beta} \right)^{\eta} \sigma_i^{\circ}. \tag{14}$$

Given $\sigma^{\alpha\beta,\circ}$, the energetic contributions from either phase at the liquid–liquid interface may be estimated by applying Antonov's rule separately to each monolayer adjacent to the interface, such that

$$\sigma^{\alpha,\star} = \left| \sigma^{\alpha,\mathrm{vf}} - \sigma^{\alpha\beta,\circ} \right| \qquad \text{and} \qquad \sigma^{\beta,\star} = \left| \sigma^{\beta,\mathrm{vf}} - \sigma^{\alpha\beta,\circ} \right|. \tag{15}$$

Note that the superscript vf refers to the volume-fraction-weighted mean of pure component values. The sum of these two energetic contributions $(\sigma^{\alpha,\star} + \sigma^{\beta,\star})$ yields the effective interfacial tension at the liquid–liquid interface:

$$\sigma^{\alpha\beta} = \left| \sigma^{\alpha,\mathrm{vf}} + \sigma^{\beta,\mathrm{vf}} - 2\,\sigma^{\alpha\beta,\circ} \right|. \tag{16}$$

It is important to note that an interface also exists between the exterior surface phase (which we treat as a 3-D Guggenheim interfacial phase) and the interior bulk of a particle (see Fig. 1 for details). This interface, henceforth referred to as the bulk–surface interface, can be treated in much the same way as the liquid–liquid interface between phases α and β using any of the approaches outlined in Table 1. This "ls" interface contributes an additional energetic term, which scales with σ^{ls}, to the overall Gibbs energy of the particle in addition to the interfacial tension contribution that scales with $\sigma^{\alpha\beta}$. While the energetic contribution from this boundary is likely small, it cannot be neglected categorically, since differences in composition between the surface phase and the adjacent bulk phase may become significant, especially at higher RH, at which the particle is well-mixed or phases α and β similar in composition. At intermediate and lower relative humidities in the presence of LLPS, the compositions of phases α and β tend to be more distinct from each other. Under those conditions it is likely that the α–β LL interface plays a larger role than the bulk–surface interface (see Fig. 3). The area of the bulk–surface interface can be calculated as follows:

$$A^{\mathrm{ls}} = 4\pi \left(r_p - \delta^{\mathrm{s}} \right)^2. \tag{17}$$

The value of σ^{ls} can be calculated using the same approaches as for $\sigma^{\alpha\beta}$. For consistency, we always apply the same method to both interfaces for a given case. Refer to Table 1 for a summary of the various interfacial tension approaches applied in this work.

An important feature of σ^{ls} is that it cannot be fully disentangled from σ^{s} as expanding the surface of a solution droplet will expand both the boundary at the gas–liquid interface as well as the boundary between the bulk phase and the surface phase. Therefore, the expression for the chemical potential of the surface phase as described in Schmedding and Zuend (2023) must be modified slightly when accounting for this additional interface. An exception is the case of a pure-component droplet, in which case $\sigma^{\mathrm{ls}} = 0$.

The following equations define the component-specific and interface-aware chemical potentials in the surface phase and an adjacent liquid bulk phase (Aston and Herrington, 1991):

$$\mu_i^{\mathrm{s}} = \mu_i^{\circ,\mathrm{s}} + RT \ln\left(a_i^{\mathrm{s}}\right) + \sigma_i^{\circ} \mathscr{A}_i^{\mathrm{s}} - \sigma^{\mathrm{s}} \mathscr{A}_i^{\mathrm{s}};$$ (18)

$$\mu_i^{\mathrm{b}} = \mu_i^{\circ,\mathrm{b}} + RT \ln\left(a_i^{\mathrm{b}}\right) - \sigma^{\mathrm{ls}} \mathscr{A}_i^{\mathrm{b}}.$$ (19)

Equation (19) describes the chemical potential of components (i) in a liquid bulk phase when additionally accounting for the contributions of i to the 2-D LL interfacial energy per unit amount of substance of the ls interface. Equations (18) and (19) may be combined under equilibrium conditions ($\mu_i^{\mathrm{b}} = \mu_i^{\mathrm{s}}$) while assuming (defining) that $\mu_i^{\circ,\mathrm{s}} = \mu_i^{\circ,\mathrm{b}}$. This leads to a coupled expression for the surface tension at the gas–liquid interface:

$$\sigma_i^{\mathrm{s}} = \frac{RT}{\mathscr{A}_i^{\mathrm{s}}} \ln\left(\frac{a_i^{\mathrm{s}}}{a_i^{\mathrm{b}}}\right) + \sigma_i^{\circ} + \sigma^{\mathrm{ls}} \frac{\mathscr{A}_i^{\mathrm{b}}}{\mathscr{A}_i^{\mathrm{s}}}.$$ (20)

An alternative, mathematically equivalent option is to fold the effect of an LL interface into adjusted bulk phase activities ($a_i'^{,\mathrm{b}}$), as described in Section 2.3.

2.3 Coupled Vapor–liquid–liquid and bulk–surface equilibrium calculation

Using the coupled vapor–liquid–liquid equilibrium modeling approach of Zuend et al. (2010); Zuend and Seinfeld (2012), for a given overall condensed-phase composition, a bulk liquid–liquid equilibrium (LLE) calculation is first performed while ignoring any adjustments due to bulk–surface equilibrium (BSE). This provides an initial guess in form of a condensed-phase equilibrium state for a given particle composition. Given the overall composition and particle size, an initial guess for the surface composition of the entire particle and the associated BSE problem can be generated using the initial guess algorithm of Schmedding and Zuend (2023). Rather than fully depleting species out of phase β or α, it is assumed that both phases contribute material proportionally to the total amount of surface molecules, n^{s}, such that $n_j^{\mathrm{s}} = q_j^{\alpha} \varepsilon_j n_j^{\mathrm{tot}} + (1 - q_j^{\alpha}) \varepsilon_j n_j^{\mathrm{tot}}$ where q_j^{α} is the fraction of neutral component j in phase α, $(1 - q_j^{\alpha})$ is the fraction of j in phase β, $\varepsilon_j = \frac{n_j^{\mathrm{s}}}{n_j^{\mathrm{tot}}}$, and n_j^{tot} is the total amount of species j in the liquid phases plus the surface phase while excluding any amount of species j in the gas phase. Likewise, for electrolyte component el, the contributions from phases α and β can be written as follows: $n_{el}^{\mathrm{s}} = q_{el}^{\alpha} \varepsilon_{el} n_{el}^{\mathrm{tot}} + (q_{\mathrm{lim},el}^{\alpha} - q_{el}^{\alpha}) \varepsilon_{el} n_{el}^{\mathrm{tot}}$, where $q_{\mathrm{lim},el}^{\alpha}$ is the maximum fraction of species el, which may partition into phase α. Returning to the uncoupled or 'BSE-free' calculation, these initial guess values are used for a second liquid–liquid equilibrium calculation for the interior bulk of the particle. Once a value of $\sigma^{\alpha\beta}$ is obtained, the energetic impact of the interface can be represented as an additional contribution to each component's chemical potential. In practice, this is equivalent to expressing the interfacial tension effect as an adjustment factor to the activities of components of phase α in the following form:

$$a_i'^{,\alpha} = a_i^{\alpha} \exp\left(\frac{\sigma^{\alpha\beta} \mathscr{A}_i^{\alpha}}{RT}\right).$$ (21)

Likewise, in order to accurately capture the equilibrium partial pressures, p_i, of gas-phase species over the curved droplet surface and thus the equilibrium number concentration of gas phase molecules, n_i^G, the activities of each component in the particle must be scaled by the Kelvin effect as follows:

$$S_i = a_i'^{,\alpha} \exp\left(\frac{2\sigma^s \mathscr{V}_i}{RT\,r_p}\right). \tag{22}$$

Here, $S_i = p_i/p_i^{\circ,\text{sat}}$ is the equilibrium saturation ratio and r_p is the overall particle or droplet radius. The droplet's equilibrium RH ($= S_w$) is calculated using a_w'. In the case where gas–particle partitioning of organic species is allowed, the gas-phase quantity of species i per m^3 of air, n_i^{G} is given by:

$$n_i^{\mathrm{G}} = \frac{a_i' \exp\left(\frac{2\sigma^s \mathscr{V}_i}{RT\,r_p}\right)}{p_i^{\circ,\text{sat}} V^{\mathrm{G}} RT}, \tag{23}$$

where V^{G} denotes the unit gas-phase volume ($1\ \mathrm{m}^3$).

At this point, for a given overall droplet composition and temperature and with initial guesses established for both the liquid–liquid equilibrium phase compositions (if predicted to be present) as well as the bulk–surface equilibrium and associated surface tension and interfacial tensions, we can proceed to solve the fully coupled interior phase partitioning problem of a single droplet of given size. In our present proof-of-concept implementation, which is not optimized for best computational performance, we approach this as a nested interior problem to the overall gas–particle partitioning solution as qualitatively described in the following. We run a modified version of the BSE algorithm of Schmedding and Zuend (2023) to solve the Butler equation iteratively while updating the interfacial tensions and LLE state and phase compositions. In practice, the modification is to embed the LLE refinement method by Zuend and Seinfeld (2013) to solve the LLE problem within each iteration of the parent BSE algorithm, while accounting for adjusted amounts available for phases α and β (due to changes in bulk–surface partitioning) and using interfacial-tension-adjusted activities for the components in phases α and β. This means that during each iteration within the LLE solver (and hence also within the BSE solver), the interfacial tensions are updated with the selected method (e.g. Antonov's rule or Girifalco–Good) and the normalized Gibbs energy of mixing of the droplet is updated as well. This procedure allows for a numerical solution of these coupled systems of equations within a single particle, and in conjunction with the vapor–liquid equilibrium solver (the outermost nesting level), the full equilibration of the gas phase with a population of (monodisperse) particles within a unit volume of air. It also allows for an initially assumed LLPS state (for the corresponding bulk system) to disappear if it becomes unfavorable due to bulk–surface partitioning and interfacial tension impacts on adjusted component activities.

In summary, a coupled system of nonlinear algebraic equations needs to be solved, the solution of which must fulfill the necessary condition that the interface-corrected activities (a_i') are equivalent across all phases at equilibrium. These corrected activities can be employed along with the relative molar amounts in each phase to determine the change in Gibbs energy due to mixing and interfaces per mole of particulate matter (G^{PM}) for a given particle radius, r_{p}. The following expanded equation

is employed:

$$G^{\mathrm{PM}} = \frac{1}{n^{\mathrm{PM}}} \left(\sum_j \left(n_j^\alpha RT \ln a_j^{\prime;\alpha} \right) + \sum_j \left(n_j^\beta RT \ln a_j^{\prime;\beta} \right) + \sum_j \left(n_j^{\mathrm{s}} RT \ln a_j^{\prime;\mathrm{s}} \right) + \sum_j \left(n_j^{\mathrm{PM}} \frac{2\sigma^{\mathrm{s}} \mathscr{V}_j}{r_{\mathrm{p}}} \right) \right) \tag{24}$$

285 where n_j^{PM} represents the moles of j in the particulate matter (any condensed phase) and $n^{\mathrm{PM}} = \sum_j n_j^{\mathrm{PM}}$. Note that this equation only applies to a monodisperse aerosol population.

3 Results

At the boundary between two distinct phases there exists an energetic penalty. In the case of a gas–liquid boundary, this penalty is often referred to as the surface tension. A similar tension exists at the boundary between two liquid phases. If the gas–liquid

290 interface can be thought of as a finite-depth region, with a distinct composition from the adjacent liquid phase beneath it, then there must exist an interfacial tension at this boundary as well. The sum of this interfacial tension and the surface tension at the gas–liquid boundary form the measurable surface tension that can be observed directly. Numerous methods have been proposed to determine the interfacial tension between two liquid phases using thermodynamic theory and semi-empirical approaches and system-specific fits. The sum of the three energetic interfacial contributions lead to differences in the total Gibbs energy for a

295 well-mixed or phase-separated particle. Greater differences in Gibbs energy occur in particles with higher surface/interfacial-area-to-volume ratios. Such differences in Gibbs energy may be sufficiently large that they lead to reductions in the onset RH of LLPS or even the complete suppression of LLPS.

3.1 Interfacial and surface tensions

Throughout this study we presume that both $\sigma^{\alpha\beta}$ and σ^{ls} can be determined using one of the introduced methods. Several of

300 those methods rely on the assumption that hypothetical gas–liquid surface tensions of the phases involved can be estimated based on a weighted average of the pure-component surface tensions, σ_i°. In order to explore the validity of this assumption, volume-fraction-based and mole-fraction-based approaches for estimating the surface tension are compared to experimental surface tension data. Figure 2 shows the predicted surface tensions using the aforementioned weighted average approaches based on the composition of the surface and bulk phases as determined by the bulk–surface partitioning treatment of Schmed-

305 ding and Zuend (2023) along with the more thermodynamically rigorous treatment of surface tension from that same work. It is shown that all three approaches can reasonably approximate the measured surface tensions of the finite volume droplets, with the volume-fraction-based approach performing better than the mole-fraction-based approach for the water and ethanol system. Both weighted average approaches give similar results for the aqueous NaCl system.

To compare the relative magnitudes of the different approaches laid out in this work, a 1000 nm dry diameter water–PEG-

310 400–ammonium-sulfate system was modeled with each of the four approaches described in Sections 2.1 and 2.2. The potential crystallization (efflorescence) of ammonium sulfate at lower RH was ignored in our model calculations, hence rendering

predictions for RH $<\sim 35\,\%$ rather hypothetical, but allowing us to perform and interpret calculations over a wide range in electrolyte concentrations. Shown in Fig. 3 are the values of $\sigma^{\alpha\beta}$, σ^{ls}, σ^{s}, and $\sigma^{\mathrm{s}\star}$ for each of the aforementioned approaches. Antonov's rule (Eq. 1, panel A) leads to the largest predicted values of $\sigma^{\alpha\beta}$ and σ^{ls} along with the smallest σ^{s}. The other three

315 approaches have minimal effects on σ^{s}, except near the onset of phase separation. In these panels of Fig. 3, when viewed from high to low RH, the onset of LLPS is the reason for the visible and related kinks in the σ^{ls} and σ^{s} curves, as well as the more obvious onset of nonzero $\sigma^{\alpha\beta}$ values. The weighted mean approach (panel D) exhibits unique behavior with a local maximum of $\sigma^{\alpha\beta}$ at $\sim 50\,\%$ RH and a local minimum at $\sim 10\,\%$ RH. Such behavior may be caused by the compositions of phases α and β becoming more similar as water is removed from the system and other organic species become dominant as solvents.

320   Given the lack of interfacial tension data for atmospherically relevant aerosol systems, it is difficult to compare any of the approaches laid out in this work to direct measurements for validation. However, Song et al. (2013) reported interfacial tension values near the onset of liquid–liquid phase separation for a bulk water–PEG-400–ammonium sulfate system. Shown in Fig. 4A are these measurements in comparison to Antonov's rule (Eq. 1), the Girifalco–Good equation (Eq. 2), the Butler equation with geometric mean activity coefficients (Eqs. 9 and Eq. 11), and the weighted mean approach developed in this work (Eq. 16).

325 For this system, which only included measurements near the onset of phase separation, Eq. (9) best matches the measured interfacial tension followed by Eq. (2), while Eq. (1) performs most poorly. It should be noted that adjusting the value of ϕ in Eq. (2) may lead to a better match with measured data; however, use of such adjusted parameters requires refitting of ϕ for each specific system and thus reduces the predictive power and application of the model. Figure 4B shows the predicted interfacial tensions from a water–benzene–sodium-chloride system along with bulk solution measurements as a function of

330 sodium chloride concentration in the salt-rich aqueous phase. In this case, none of the models described in this work are capable of reasonably matching the measurements, with Antonov's rule performing the best and the other approaches yielding substantially lower interfacial tensions, including at zero NaCl content. Similarly, Fig. 4C, shows measured and predicted interfacial tensions for a water–dodecane–potassium-chloride system as a function of the aqueous phase electrolyte molality. In this case, Antonov's rule performs the best of the various approaches and is capable of closely matching the measured

335 interfacial tension at high electrolyte concentrations, while all of the other approaches fail to capture the measured behaviour. Finally, measurements of an electrolyte free system of water–benzene–methanol is shown in Fig. 4D. At high methanol mole fractions, the measured interfacial tensions are most similar to those predicted by the weighted mean approach, while the Butler equation based approach underpredicts the interfacial tension, but performs the second best. At low methanol content, Antonov's rule is again the best method for this nearly completely phase-separated system (as in Fig. 4B). In order to better

340 understand the importance of σ_i° in determining the value of $\sigma^{\alpha\beta}$ and σ^{ls}, predictions corresponding to those shown in Fig. 4 were performed with adjustments to $\sigma_{\mathrm{org}}^\circ$ and $\sigma_{\mathrm{el}}^\circ = \sigma_{\mathrm{w}}^\circ$; those are shown in Fig. S1. Briefly, minor adjustments to σ_i° lead to better agreement between the Girifalco-Good equation and measured data fro the water–PEG-400–ammonium-sulfate system in panel A. In panels B and C, there is better agreement between Antonov's rule and the water–benzene–sodium-chloride system and the water–dodecane–potassium-chloride system with the adjustments to σ_i°. However, in panel D, Antonov's rule

345 performs more poorly for the interfacial tension in comparison to measurements for the water–benzene–methanol, assuming the same values of benzene and methanol as those in panels B and C of Fig. S1.

Equation (2) contains a single semi-empirical fit parameter, ϕ, which grants it some degree of flexibility at the expense of predictive power. Harris and Byers (1989) reported that fitted values of ϕ lie between approximately 0.55 and 1.15 for many systems. Note that, as previously in section 1, it is assumed that $\phi = 1$ when an interface-free LLE calculation predicts a

350 homogeneously mixed particle. If this were not the case then non-zero interfacial tension values between two identical phases would be possible. Thus ϕ is allowed to deviate from it's default value of 1.0 when the interface-free LLE calculation predicts phase separation. Shown in Fig. 5 are the values of the predicted LL interfacial tensions when ϕ is varied over the range of 0.55 to 1.15 for a water–suberic acid–ammonium-sulfate system. Values of ϕ greater than 1 can produce unrealistically small $\sigma^{\alpha\beta}$ values (including negative interfacial tensions), while $\phi < 1$ increases $\sigma^{\alpha\beta}$ values. Overall, the tested range in values of

355 ϕ from 0.55 to 1 results in a relatively wide range of physically feasible outcomes for the shown system, e.g. spanning about $70 \ \mathrm{mJ \, m^{-2}}$ in $\sigma^{\alpha\beta}$ at $80\,\%$ RH. Hence, optimizing this parameter for a specific system could be a successful approach for achieving a close match to measurements, especially if a composition dependence is also considered. However, such a tuning approach is inconsistent with a typical goal in atmospheric aerosols modeling, namely that of developing generally predictive methods (here of interfacial tension) applicable to a wide range of multicomponent aerosol systems and independent of any

360 experimental data required for specific tuning purposes.

3.2 Size-dependent phase separation in core–shell aerosols

Figure 6 shows the predicted and normalized mole fraction of water in the ammonium-sulfate-rich phase α ($x_w^\alpha / x_w^{\alpha,\text{no IFE}}$) for water–PEG-400–ammonium sulfate particles using the four treatments for interfacial tension laid out in this work. (see figures S2 and S3 in the SI for the plots corresponding to the normalized mole fractions of PEG-400 and ammonium sulfate in phase

365 α). In order to better understand the role of interfacial energy in terms of its feedback on particle phase compositions, the shown mole fractions are normalized by those predicted by the no IFE treatment for the same conditions. Even at RH values above the onset of LLPS, where only σ^{ls} affects the composition of the single liquid phase (α) present, there is a reduction in the concentration of water relative to the no IFE case. That is, the values of $x_w^\alpha / x_w^{\alpha,\text{no IFE}}$ are consistently ≤ 1.0, indicating a reduction in the relative water content of phase α when $\sigma^{\alpha\beta}$ and σ^{ls} are accounted for. This indicates that interfacial tension

370 effects in aerosols are not only of importance for shifting the onset in LLPS or for cloud droplet activation, but that they also impact the equilibrium compositions of the various particle phases, unlike in macroscopic bulk systems (for which the no IFE case is a better proxy). At lower RH values, the difference in composition is more pronounced, as all four approaches lead to differences of an order of magnitude from the interfacial energy-free treatment. With each approach there was also a noticeable dependence on particle dry diameter. For the 10 nm particles, these differences in composition are most substantial, while

375 the 1000 nm particle and the 100 nm particle behaved more similarly to one another. In Fig. 6A, the 10 nm particle exhibits complete suppression of LLPS, across the entire RH range. However, all other interfacial tension treatments lead to LLPS in a certain RH range, as marked by the sudden change (kinks) in $x_w^\alpha / x_w^{\alpha,\text{no IFE}}$ with decreasing RH.

Figure 7 shows the equilibrium water vapor saturation ratio (i.e. RH) corresponding to the onset of liquid–liquid phase separation (also denoted as SRH) for: (A) a water–PEG-300–ammonium-sulfate system and (B) a water–1,2,6-hexanetriol–

380 ammonium-sulfate system, both corresponding to systems examined by Ohno et al. (2023); (C) a 12-component complex

SOA surrogate mixture (CSOA) with succinic acid mixed with water and ammonium sulfate and (D) a water–α-pinene-SOA–ammonium sulfate system. (C) and (D) correspond to systems studied experimentally by Kucinski et al. (2019). The α-pinene SOA surrogate system used here for the model predictions is based on the components and relative compositions tabulated by Rastak et al. (2017). Shown for each system are the impacts of the four interfacial tension estimation approaches on the separation RH of LLPS: $\sigma^{\alpha\beta} = 0$, Eq. (1), Eq. (2), and Eq. (9). For all systems, applying Eq. (1) led to the most substantial reductions in the onset RH of LLPS, with noticeable decreases in the separation RH occurring in particles with wet diameters between approximately 100 nm and 250 nm. In the case where $\sigma^{\alpha\beta} = 0$, our model predicts an increase in the separation RH for small particle sizes, caused mostly by an increase in effective equilibrium RH at small particle diameters due to the Kelvin effect. It should also be noted that the consideration of nonzero σ^{ls} encourages the occurrence of LLPS and shifts the onset of LLPS in smaller particles to higher RH values as compared to particles with the same initial composition but a larger dry diameter. Indeed, relative to said larger particles, there is a slight increase in the separation RH values in the sub-100 nm (wet diameter) size range for the water–PEG-300–ammonium sulfate system, while a more noticeable decrease in separation RH is predicted for particles with diameters < 20 nm. In comparison to observations of size-dependent LLPS behavior, Antonov's rule is the only approach that is consistently capable of suppressing phase separation to below $20\,\%$ RH for small wet diameters (likely reported as complete suppression in measurements) for all of the systems shown. The application of Antonov's rule also leads to measurable decreases in the onset RH of LLPS even for relatively large particle wet diameters (> 200 nm), in agreement with the experimental data reported by Ohno et al. (2023) and Kucinski et al. (2019). Indeed, for the α-pinene SOA system shown in Fig. 7D, only Antonov's rule leads to a notable size dependence in the LLPS onset RH. The corresponding values of $\sigma^{\alpha\beta}$ at the onset of LLPS are shown in Fig. S2 and the water-free OIRs are listed in Table S3. For treatments which predict stronger size-dependencies on the separation RH, there is less agreement between $\sigma^{\alpha\beta}$ at the onset of LLPS for the weighted mean interfacial composition approach. This is due to the fact that the predicted $\sigma^{\alpha\beta}$ exhibits a local minimum at low RH values (see fig. 3D). The location of such a local minimum is a function of particle size and thus smaller particles may undergo LLPS at RHs below the RH which minimizes $\sigma^{\alpha\beta}$.

Figure S4 shows the value of $\sigma^{\alpha\beta}$ at the SRH for the systems shown in Fig. 7. For all systems, $\sigma^{\alpha\beta}$ at the SRH is lower for larger particles and begins to increase with decreasing particle size. This is due to the fact that these particles experience a decrease in the SRH and therefore the compositions of phases α and β become more distinct at the SRH. However, it should be noted that for very small particles the value of $\sigma^{\alpha\beta}$ at the SRH begins to decrease. Said trend is most clear when Antonov's rule is applied. This decreasing trend suggests that the compositional differences between liquid phases at very small sizes and low RH become less distinct as the overall water content of the particle is low. Such a trend may be responsible for the behavior shown in Fig. 7B and C, wherein the smallest particles do not neatly decrease in SRH with respect to particle size; indeed, the competing effects among $\sigma^{\alpha\beta}$, σ^{ls}, and $\sigma^{s,\star}$ lead to weaker decreases in SRH and in the case of panel C and either Eq. (2) or Eq. (9) treatment, a plateauing effect with a local maximum and then a continued decrease in SRH. However, this effect is small relative to the overall decrease in SRH with decreasing particle size.

Figure S5 shows the same systems as in Fig. 7, but with the assumption that $\sigma^{\mathrm{ls}} = 0$. For the more extreme treatments of $\sigma^{\alpha\beta}$, such as with Antonov's rule or the weighted mean composition approach, the exclusion of σ^{ls} has a negligible impact on the

size-dependent SRH. However, if $\sigma^{ls} = 0$ and a less extreme treatment of $\sigma^{\alpha\beta}$, such as the Girifalco–Good equation (Eq. (2)) or Eq. (9) is used, then there is a positive increase in the SRH that is very similar to the No IFE case. It is also important to note that the local maximum behavior discussed in Figure 7 is still present and thus cannot be attributed to the presence or absence of σ^{ls}. Employing either Eq. (2) or Eq. (9) yield quantitatively similar LLPS behavior. This suggests that the Girifalco–Good

420 equation (Eq. 2) may serve as a good approximation of a more thermodynamically rigorous treatment for the LL interface – at least for qualitatively similar systems to the ones studied in this work.

For particles of less than 100 nm in (wet) diameter, the hypothetical minimum LL interfacial tension necessary to fully suppress LLPS, $\sigma_{\text{suppr}}^{\alpha\beta}$, was calculated based on the difference between the predicted molar Gibbs energy of the phase-separated solution and that of the homogeneous solution in the No IFE case. These values are shown in Fig. 8 for the systems from Fig. 7.

425 Both the water–PEG-300–ammonium-sulfate and the water–1,2,6-hexanetriol–ammonium-sulfate systems exhibited weaker size dependence for $\sigma_{\text{suppr}}^{\alpha\beta}$ than the water–CSOA-with-succinic-acid–ammonium-sulfate system, and the water–α-pinene-SOA–ammonium-sulfate system. At low RH ($< 30\%$), both of these SOA-proxy systems required large (> 100 mJ m^{-2}) $\sigma_{\text{suppr}}^{\alpha\beta}$ values to inhibit LLPS, even in the ultrafine size regime. As expected, at RH levels near the onset of phase separation, very small values of $\sigma^{\alpha\beta}$ already exceed $\sigma_{\text{suppr}}^{\alpha\beta}$ in case of all systems. However, the systems shown in Fig. 8 do not include

430 any feedback from the inclusion of σ^{ls} treatments. The different treatments for σ^{ls} lead to differences in the composition of the particle before the onset of phase separation and as such, may lead to modifications to the value of $\sigma_{\text{suppr}}^{\alpha\beta}$ for the systems shown. The comparison and size effects shown in Fig. 8 mainly serve the purpose of demonstrating that a size dependence exists, yet that complete suppression of LLPS in the RH range from 40% to 80% is energetically rather difficult (at least when assuming that AIOMFAC reasonably represents the molecular interactions).

435 **4 Discussion and atmospheric implications**

The approaches for predicting LL interfacial tension described and tested in this work can produce a broad range of values for the a system under otherwise the same conditions. For mixtures in which there is a higher degree of mutual solubility among components preferring either phase α or β, e.g., the water–PEG-300–ammonium-sulfate, water–PEG-400–ammonium-sulfate, water–1,2,6-hexanetriol–ammonium-sulfate, and the water–benzene–methanol systems, the Girifalco–Good equation and the

440 Butler equation with geometric mean activity coefficients (Eq. 12) agree well with previously reported experimental data. In the case of systems with more complete phase separation, such as the water–benzene–NaCl system and the water–dodecane–KCl system, Antonov's rule appears to be an appropriate method. It is important to note that such systems exhibiting nearly complete phase separation are not necessarily representative of atmospherically relevant systems that may be found in ambient mixtures of water, SOA and inorganic ions (Zuend et al., 2011).

445 The inclusion of interfacial energy corrections mapped onto the chemical activities of components in affected particles can be important for the resulting equilibrium particle phase compositions, even of larger particles, as shown in Fig. 6. The effects are more pronounced for smaller particles; however, the magnitude of the change in composition in comparison to the No IFE case is approximately the same for the four approaches of interfacial energy prediction discussed in this work.

Despite better agreement with interfacial tension measurements, the application of the Girifalco–Good equation and the

450   Butler equation with geometric mean activity coefficients do not agree well with observed separation relative humidities as a function of particle size. Indeed, Antonov's rule is the only approach which consistently predicts size-limited phase separation for the systems examined in this work. Importantly, the application of Antonov's rule to the systems examined in Ohno et al. (2023) leads to relatively good agreement with the observed size-dependent reduction in separation RH for both the water–PEG-300–ammonium-sulfate and the water–1,2,6-hexanetriol–ammonium-sulfate systems. We note that the No IFE simulations

455   lead to higher separation relative humidities for larger particles in both cases. However, in the case of the water–PEG-300–ammonium-sulfate system, Ohno et al. (2023) discuss limiting the upper bound of the explored RH range in their experiments to 83% to avoid issues with condensation in their setup.

For the complex SOA system with ammonium sulfate analyzed by Kucinski et al. (2019), the application of Antonov's rule leads to a predicted reduction in SRH; however, only particles with diameters below 20 nm exhibited complete suppression of

460   phase separation. Likewise, the α-pinene SOA surrogate system only exhibited complete suppression of LLPS for particles with diameters below 15 nm. For this system, the components were based on those generated by the Master Chemical Mechanism for a specific ozonolysis case study (Rastak et al., 2017); therefore, most of the used $\sigma_{\mathrm{org}}^{\circ}$ values were not available from measurements and we assumed a value of 35 mJ m^{-2} for those organic products. It is possible that better constraints on these values may lead to larger $\sigma^{\alpha\beta}$ values, which are capable of further suppressing LLPS at higher relative humidities. However, for

465   this system the interfacial tension required to suppress LLPS becomes quite high as the RH decreases. It is therefore unlikely that realistic interfacial tensions of typically less than 100 mJ m^{-2} will completely inhibit LLPS across the full RH range for all but the smallest ultrafine particles.

The energetic contributions of the LL interface and the bulk–surface interface have competing effects on a particle's internal mixing state. If an energetic contribution from the LL interface is included and the bulk–surface interface is neglected then

470   particles may exhibit decreases in SRH. However, if both contributions are included and assuming that the same treatment is used for both interfaces (e.g., Eq. 2) then particles with smaller diameters phase-separate at the same or higher relative humidities than larger particles in all but the most extreme cases of interfacial tension. This is likely due to the fact that in a particle in which phase separation is suppressed (compared to the macroscopic bulk case), the composition of the surface will be more distinct from that of the interior bulk, leading to a larger energetic contribution at the bulk–surface interface. Given that

475   the area of the bulk–surface interface must inherently always be larger than the $\alpha\beta$ LL interface, a comparable bulk–surface LL interface value would lead to a larger total energetic contribution per particle. Thus, in many cases it becomes favorable even for an ultrafine particle to form a LLPS and thereby substantially lower σ^{ls} while introducing a nonzero $\sigma^{\alpha\beta}$.

The inclusion of surface energy, liquid–liquid interface, and bulk–surface interface may also lead to a more complete picture regarding the structure of the surface phase. Thicker 3-D surface phases of larger corresponding δ^{s} values typically imply

480   higher surface energy contributions. However, surfaces with thicker δ^{s} values tend to be of compositions that are more similar to the interior bulk of the particle. This would reduce the energetic penalties from the bulk–surface interface and inhibit phase separation by increasing depletion of species out of the interior bulk of the particle to the surface phase. Likewise, the opposite effects likely would occur in a particle with a surface that has a small δ^{s} value. The particle would have a lower surface

energy coupled with a higher bulk–surface LL interfacial tension and reduced inhibition of LLPS. To explore this trade-off

485   quantitatively, we have run a range of predictions during which δ^s was allowed to vary from 0.1 to $17.5\,\mathrm{nm}$ in surface thickness and evaluated the resulting normalized Gibbs energy of the system. Simulations were not conducted above $\delta^\mathrm{s} > 17.5\,\mathrm{nm}$ as this would represent an extreme case wherein the volume of the surface could become substantially greater than the volume of phase β. Figure 9 shows the determined optimum values of δ^s for a water–1,2,6-Hexanetriol–ammonium sulfate particle with a water-free diameter of $250\,\mathrm{nm}$ as function of RH. For this system, the optimum δ^s value ($\delta^\mathrm{s}_\mathrm{best}$) is calculated for the various

490   interfacial tension options for $\sigma^{\alpha\beta}$ and σ^ls compared throughout this work: the No IFE case, Antonov's rule (Eq. (1)), the Girifalco-Good equation (Eq. (2)), the Butler equation with geometric mean activity coefficients (Eq. (12)) and the weighted mean interfacial composition approach (Eq. (16)). As the relative humidity is decreased, the thickness of $\delta^\mathrm{s}_\mathrm{best}$ increases near the onset of LLPS. Values of $\delta^\mathrm{s}_\mathrm{best}$ remain high and then decrease in all cases. In the case of the weighted mean interfacial composition approach (Eq. (16)), the decrease in $\delta^\mathrm{s}_\mathrm{best}$ is more gradual at lower RH. The application of Antonov's rule leads

495   to unique behavior among the different methods tested, due to it's suppression of LLPS when δ^s is large. This causes $\delta^\mathrm{s}_\mathrm{best}$ to return to large values at lower RHs which forces the particle to form a single bulk phase with a very thick surface phase. Such behaviour is due to the particle trying to minimize compositional differences across phases α, β, and the surface by increasing the material present in the surface phase. The relative changes $\delta^\mathrm{s}_\mathrm{best}$ with decreasing RH near the onset of phase separation are similar in magnitude for the no IFE case, the Girifalco–Good equation, the Butler Equation with geometric

500   mean scaled activity coefficients, and the weighted mean interfacial composition approach. Such behavior suggests that the inclusion of bulk–surface partitioning is more important for determining the structure of the surface phase than the inclusion of σ^ls. At RH values further below the onset of LLPS $\delta^\mathrm{s}_\mathrm{best}$ becomes much smaller again for the no IFE case, the Girifalco–Good equation, the Butler Equation with geometric mean scaled activity coefficients, approaching the physical limit of a three-dimensional surface phase ($\delta^\mathrm{s}_\mathrm{best} = 0.1\,\mathrm{nm}$) in agreement with Schmedding and Zuend (2023). This is likely due to the fact

505   that the energetic contributions of $\sigma^{\alpha\beta}$ are much larger than those of σ^ls and that lower values of δ^s correspond to lower values of $\sigma^{\mathrm{s}\star}$. The results reported by Schmedding and Zuend (2023), which did not account for the energetic penalty of the bulk–surface interface, found that thinner surfaces are more energetically favorable for well-mixed particles. The inclusion of this interfacial contribution suggests that the most favorable surface thickness is dynamic; typically favoring a thin surface phase in dilute aqueous droplets. Moreover, in some cases a thicker surface is preferred to a thinner one, especially close to the onset

510   of LLPS. This could suggest a potential mechanism wherein LLPS may occur initially as a form of bulk–surface partitioning with a gradual thickening of the surface phase before an additional distinct bulk phase forms. It is possible that such behavior may be responsible for some of the observed size-limited phase separation behavior reported in previous studies since, with limited depth resolution in an experiment, it is difficult to distinguish between a thick surface phase that is enriched in organic species and a thin, organic-rich phase β in particles in which such a configuration for the surface may be favorable.

5 Conclusions

Atmospheric aerosol particles may exhibit liquid-liquid phase separation (e.g., You et al., 2014; Huang et al., 2021). Recent observations have noted that some aerosol systems may exhibit size-dependent LLPS wherein smaller particles undergo LLPS under more extreme conditions (e.g. substantially lower RH), than large particles. This study aims to explore the interactions between phase separation, bulk–surface partitioning, and LL interfaces in aerosol particles through the extension of a previously developed bulk–surface partitioning model which now includes the coupling with a liquid–liquid phase separation model. Various treatments for the energetic contribution of LL interfaces are explored. For systems with greater miscibility among the solution components, the Girifalco–Good equation and the Butler equation more accurately reproduce measured interfacial tensions. For systems exhibiting increased immiscibility among components, Antonov's rule performs better than the other approaches. The inclusion of LL interfacial tension terms and bulk–surface partitioning leads to a predicted lowering of the separation RH of LLPS in many systems. This reduction in the separation RH was most pronounced for particles with wet diameters below 50–70 nm. The weighted mean composition approach and Antonov's rule led to the largest decreases in the predicted separation RH for all of the systems examined in this work. For the smallest particle sizes studied ($10--50$ nm in wet diameter), these two approaches lead to substantial suppression of LLPS to below 40% RH ($\sim$ efflorescence RH of ammonium sulfate) or complete inhibition of LLPS. An energetic contribution from the LL boundary between the surface phase and its adjacent bulk phase was considered in this work. This interfacial tension contribution is shown to be at its maximum near the separation RH, where the difference in composition between the surface and bulk phases is greatest.

While numerous studies have examined LLPS in larger particles and macroscopic bulk solutions, studies on LLPS in submicron-sized particles are scarce (Kucinski et al., 2019; Ohno et al., 2023; Ott and Freedman, 2020, 2021). For small particles, it can be difficult to experimentally distinguish between a surface phase of more than monolayer thickness phase and a thin bulk phase in a core–shell configuration, since the minimum required thickness to call a surface layer a "regular" liquid phase rather than a multilayer surface is a matter of perspective. The interplay of bulk–surface partitioning, interfacial tensions, and LLPS hint at the difficulties in conducting measurements on nanoparticles. Measurements of size-dependent particle properties in the submicron range should be contactless. Contact with the particle (surface) will change the surface area to volume ratio, may generate additional interfaces, induce bulk–surface partitioning feedbacks, and indirectly influence the targeted particle properties. The applicability of measurements performed on macroscopic systems for microscopic droplets needs to be considered carefully. Most LL interfacial tension measurements are made using bulk solution techniques; therefore, caution is warranted when extrapolating these data to sub-100 nm particles, for which deviations from bulk solution are pronounced. This study highlights the interest in additional measurements covering sub-100 nm particles to provide guidance for constraining model parameters. This work represents a step towards more physically realistic representations of aerosol particles accounting for LL interfaces and size-dependent LLPS behavior. While offering options for interfacial tension treatment, this model remains predictive and broadly applicable in its design. It will allow for a predictive treatment of particles in the ultrafine aerosol regime and aids in connecting measurements taken on larger particles to their smaller counterparts.

The interfacial tension at the $\alpha\beta$ interface, and the surface energies of phases α and β may be used to predict if a particle's equilibrium morphology is core–shell or partially engulfed. Because partially engulfed morphologies require additional considerations, these morphological questions are a direction for future studies.
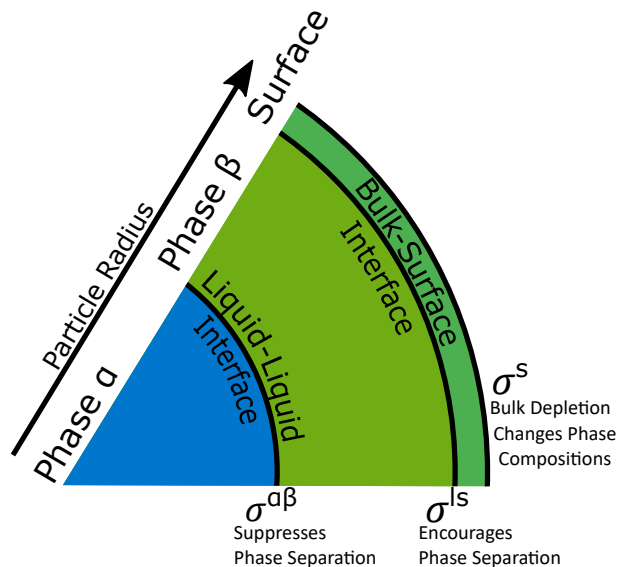
Figure 1. Schematic of phase and interface configurations considered in this study. In a liquid–liquid phase-separated aerosol particle with two liquid phases α and β, there exist two energetic penalties ($\sigma^{\alpha\beta}$ and σ^{ls}) due to interfaces between the condensed phases. There is also an energetic penalty at the gas–particle surface (σ^s). The interplay between these three energetic contributions has a feedback on the composition of particle phases and via gas–particle partitioning, the aerosol system overall.

Table 1. Summary of interfacial tension treatments used for the interfaces between phases α and β as well as between the surface phase and the liquid bulk phase just beneath it.

Name	Equation	Reference
No IFE	$\sigma^{\alpha\beta} = 0$	–
Antonov's rule	$\sigma^{\alpha\beta} = \left\lvert \sigma^{\alpha,\mathrm{vf}} - \sigma^{\beta,\mathrm{vf}} \right\rvert$	Antonov (1907)
Girifalco–Good equation	$\sigma^{\alpha\beta} = \sigma^{\alpha,\mathrm{vf}} + \sigma^{\beta,\mathrm{vf}} - 2\phi\sqrt{\sigma^{\alpha,\mathrm{vf}}\sigma^{\beta,\mathrm{vf}}}$	Girifalco and Good (1957)
Weighted mean approach	$\sigma^{\alpha\beta} = \left\lvert \sigma^{\alpha,\mathrm{vf}} + \sigma^{\beta,\mathrm{vf}} - 2\sum_i \left(\mathrm{vf}_i^{\alpha}\mathrm{vf}_i^{\beta}\right)^{\eta}\sigma_i^{\circ} \right\rvert$	This work
Geometric mean activity coefficients	$\sum_i \left[\sqrt{x_i^{\beta}x_i^{\alpha}}\exp\left(\frac{\mathscr{A}_i^{\alpha\beta}\sigma^{\alpha\beta}}{RT}\right)\right] = 1$	Bahramian and Danesh (2005)
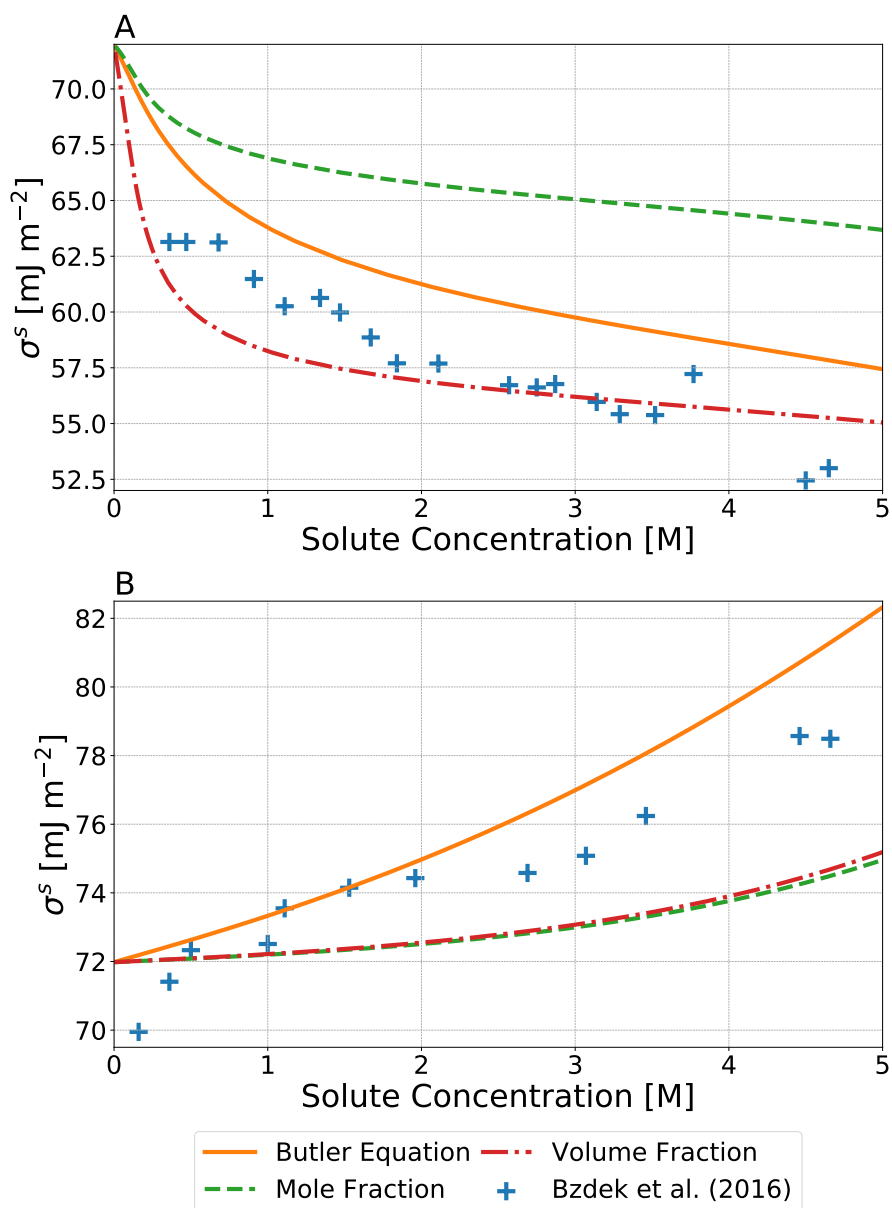
Figure 2. Predicted σ^{s} values using the Butler equation based approach of (Schmedding and Zuend, 2023), a surface phase volume-fraction-weighted mean of pure component surface tensions, and a surface phase mole-fraction-weighted mean of pure component surface tensions as a function of solute concentration for binary systems of (A) water and glutaric acid and (B) water and NaCl. The cross symbols show measurements based on the optical tweezer method by (Bzdek et al., 2016) at 298 K. Surface phase compositions were calculated using the Butler equation with the assumption that $\sigma^{\mathrm{ls}} = 0\,\mathrm{mJ\,m^{-2}}$. Bulk–surface partitioning calculations were performed assuming a water-free particle diameter of 5000 nm.
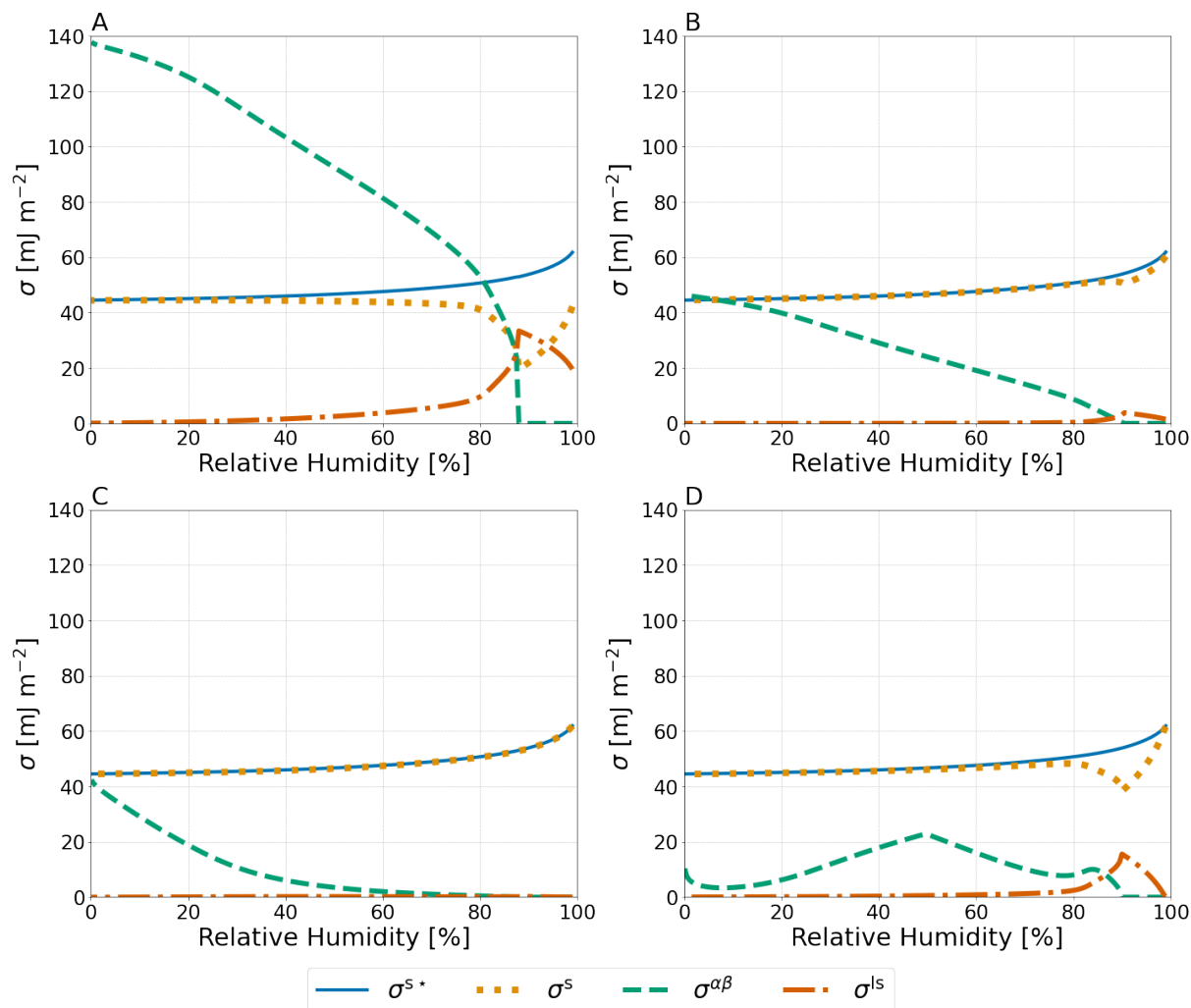
Figure 3. Predicted values of σ^{s}, $\sigma^{\mathrm{s},\star}$, $\sigma^{\alpha\beta}$, and σ^{ls} (see legend) for a particle of 1000 nm dry diameter composed of water–PEG-400–ammonium-sulfate at $T = 298$ K. $\sigma^{\alpha\beta}$ and σ^{ls} were calculated using (A) Antonov's rule (Eq. 1), (B) the Girifalco–Good equation (Eq. 2), (C) the Butler equation with geometric mean activity coefficients (Eq. 12), and (D) the weighted mean interfacial composition approach (Eq. 16).
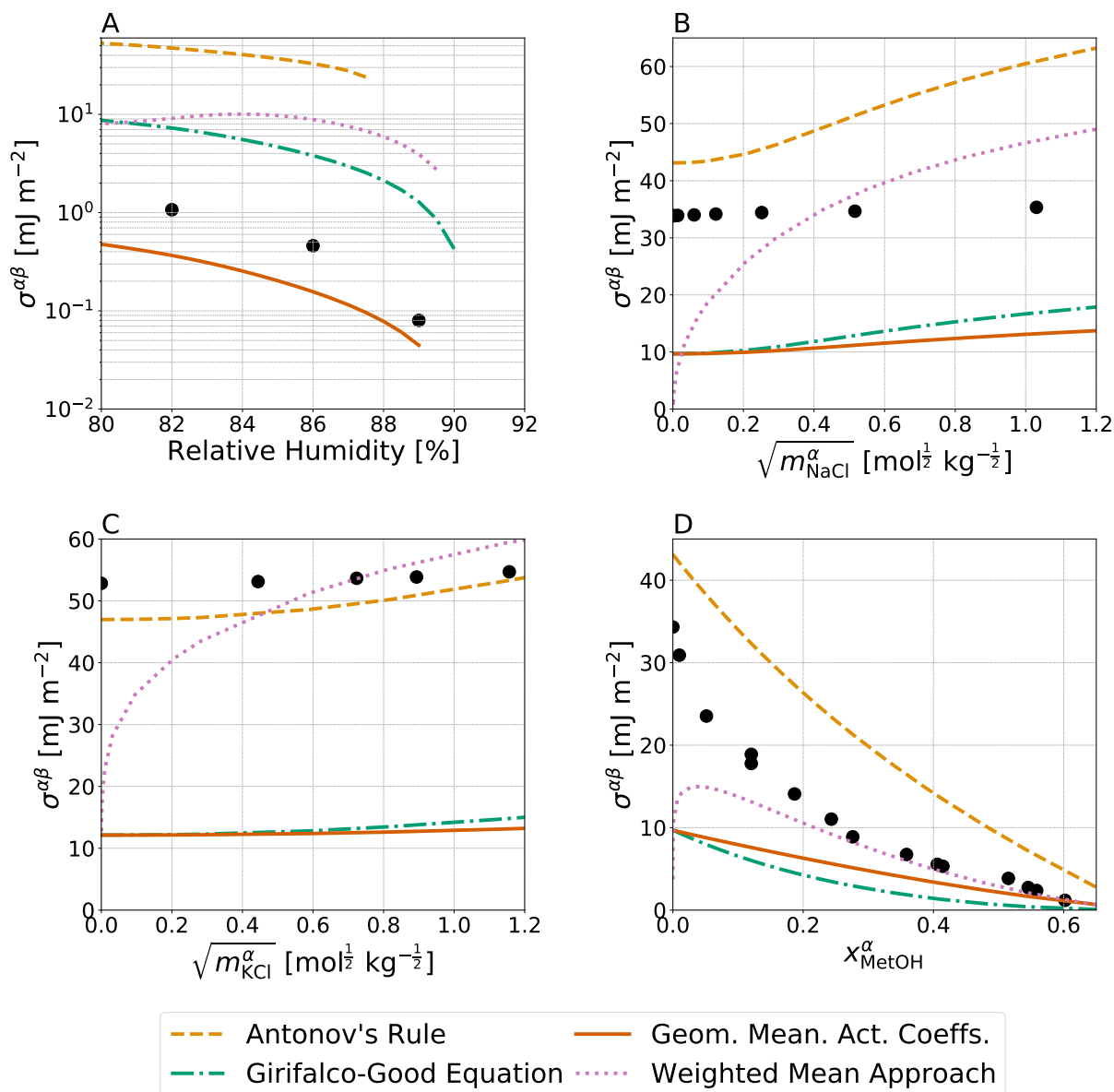
Figure 4. Predicted $\sigma^{\alpha\beta}$ values (curves) compared to measurements (solid circles). The x-axis scales correspond to those used in the experimental data references. Data and predictions for all systems are for $T = 298$ K. (A) A water–PEG-400–ammonium-sulfate system with experimental data by Song et al. (2013), (B) a water–benzene–sodium-chloride system (Harkins and Humphery, 1915), (C) a water–dodecane–lithium-chloride system (Aveyard and Saleem, 1976), and (D) a water–benzene–methanol system (Pliskin and Treybal, 1966; Paul and De Chazal, 1967). The four distinct parameterizations for interfacial tension from Table 1 are shown (except for the No IFE case). The pure-component surface tensions of organic components can be found in Table S3.
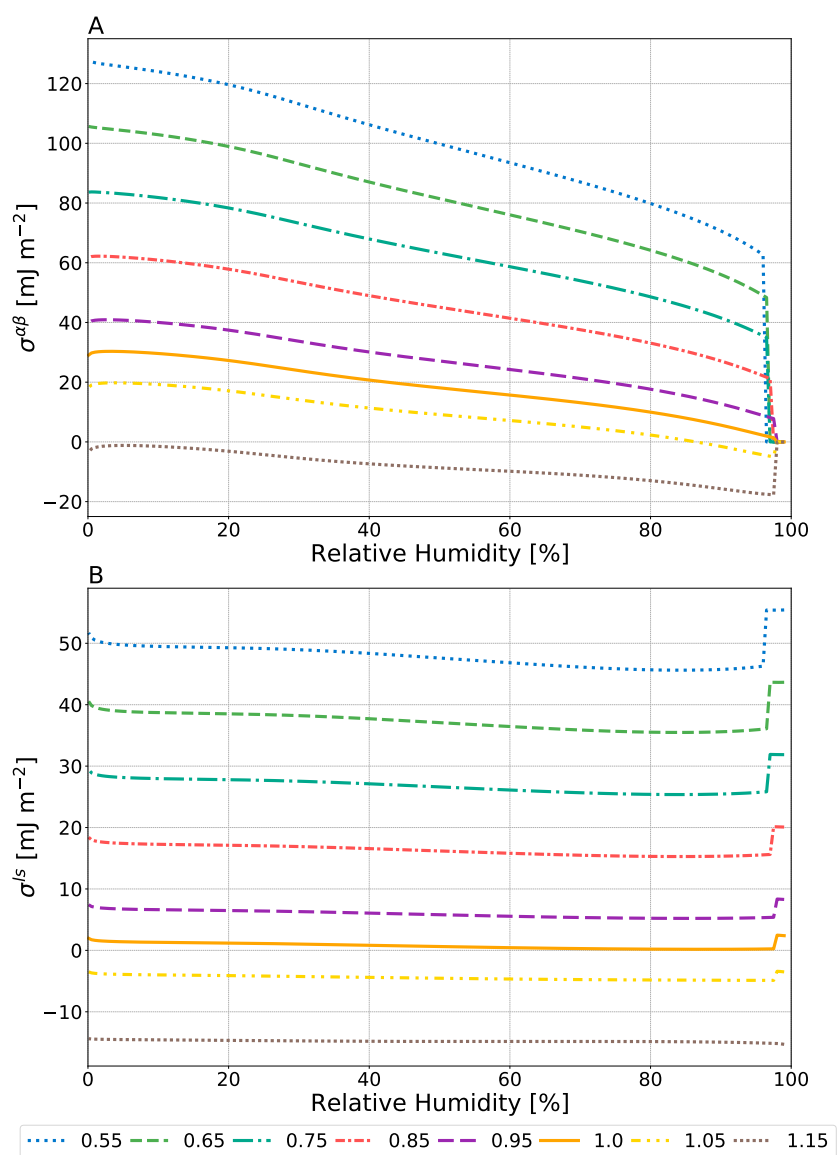
Figure 5. The effect of varying ϕ (see legend) on $\sigma^{\alpha\beta}$ of a water–suberic-acid–ammonium-sulfate particle with a water-free diameter of 1000 nm as predicted by the Girifalco–Good approach (Eq. 2). $\phi_{\min} = 0.55$ and $\phi_{\max} = 1.15$ as reported by Harris and Byers (1989).
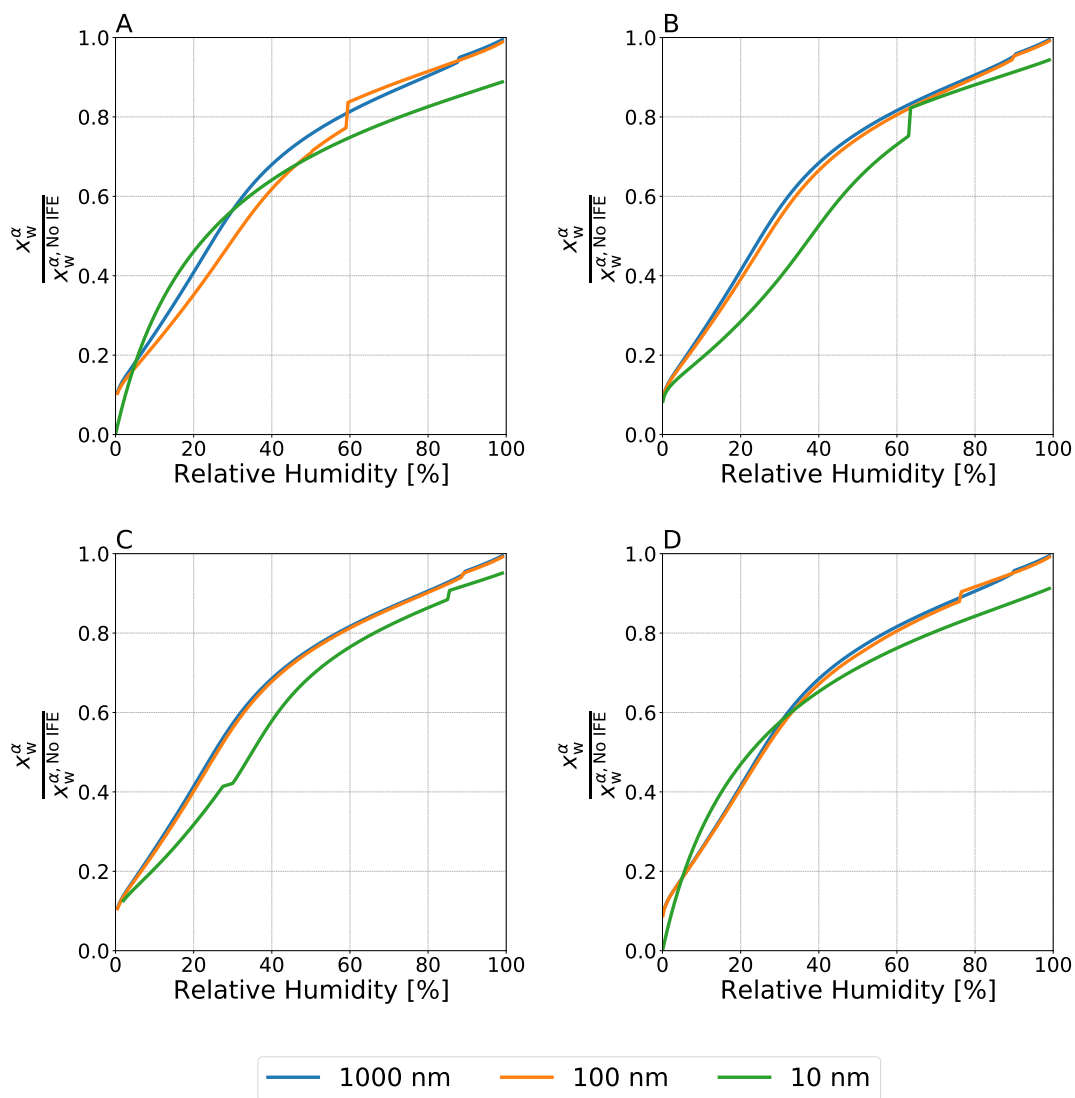
Figure 6. Normalized mole fraction of water in the aqueous phase α for water–PEG-400–ammonium sulfate particles with dry diameters ranging from 10 nm to 1000 nm at $T = 298$ K. (A) Antonov's rule, (B) the Girifalco–Good equation, (C) Butler equation with modified activity coefficients, and (D) the weighted mean interfacial composition approach. Kinks in the curves are indicative of the onset of LLPS.
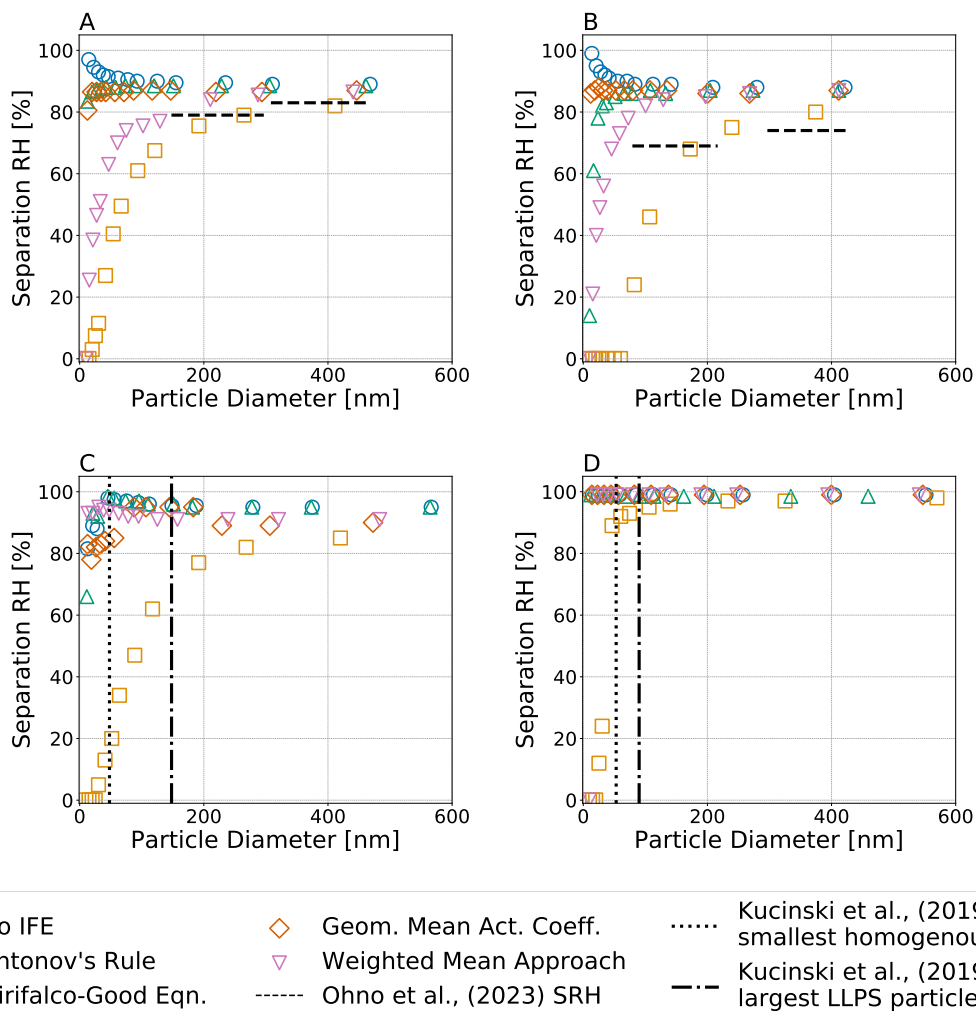
Figure 7. Predicted equilibrium separation RH versus particle wet diameter for particles of the same dry composition but different choices of interfacial tension treatment; see legend. Systems shown are: (A) water–PEG-300–ammonium-sulfate, (B) water–1,2,6-hexanetriol–ammonium-sulfate, (C) water–CSOA-with-succinic-acid—ammonium-sulfate, and (D) water–α-pinene-SOA–ammonium-sulfate. (A, B) Dashed horizontal lines indicate measured equilibrium separation RH values by Ohno et al. (2023). (C, D) Vertical lines show the observed largest homogeneous and the smallest phases-separated particles, respectively, as determined by Kucinski et al. (2019). All calculations were performed at 298 K.
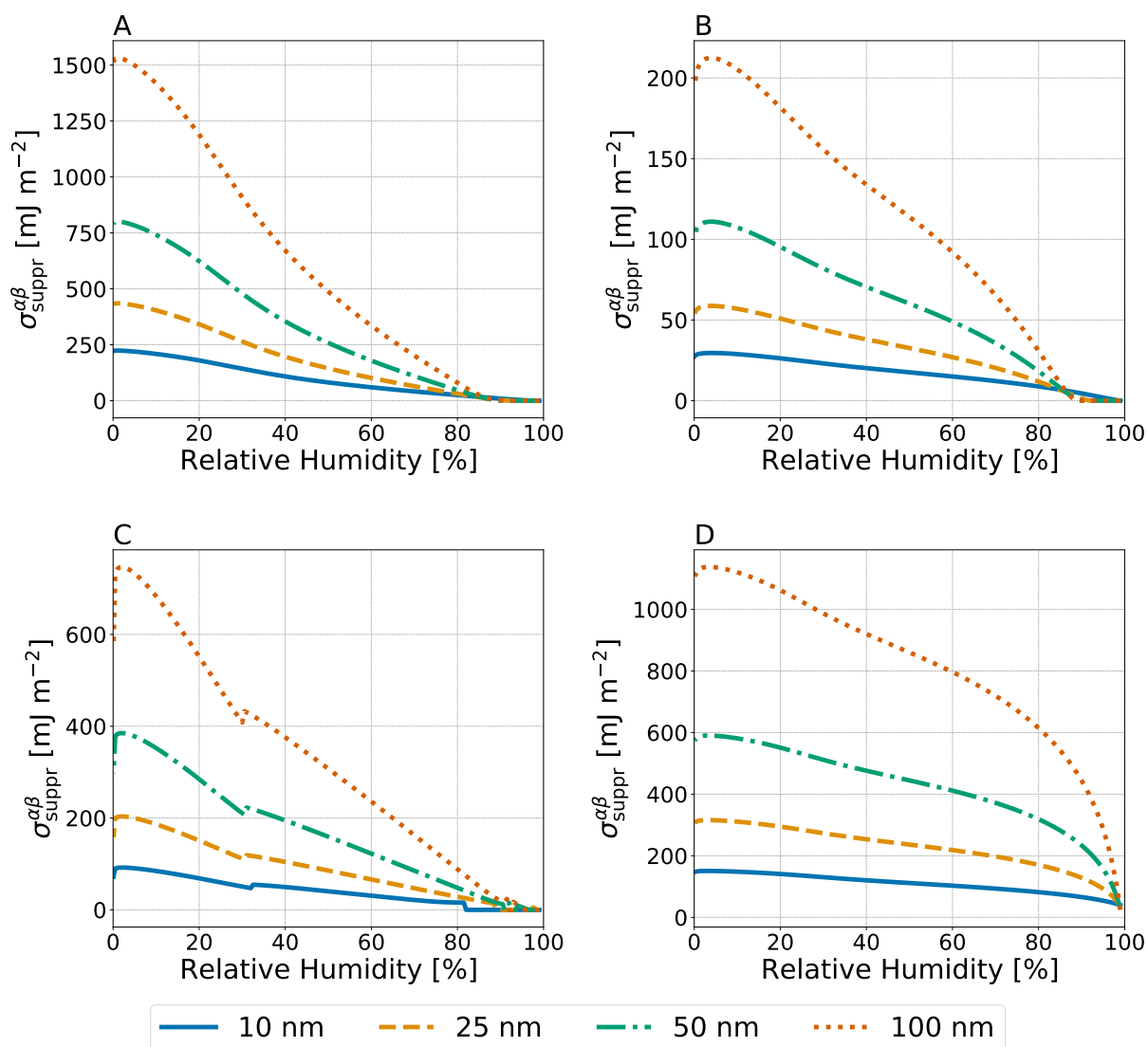
Figure 8. Predicted hypothetical $\sigma^{\alpha\beta}$ values necessary to completely suppress phase separation in the No IFE case ($\sigma^{\alpha\beta}_{\mathrm{suppr}}$) as a function of RH for particles with dry diameters of 10, 25, 50, and 100 nm (see legend) at $T = 298$ K. Systems as in Fig. 7: (A) water–PEG-300–ammonium-sulfate, (B) water–1,2,6-hexanetriol–ammonium-sulfate, (C) water–CSOA-with-succinic-acid–ammonium-sulfate, and (D) water–α-pinene-SOA–ammonium sulfate.
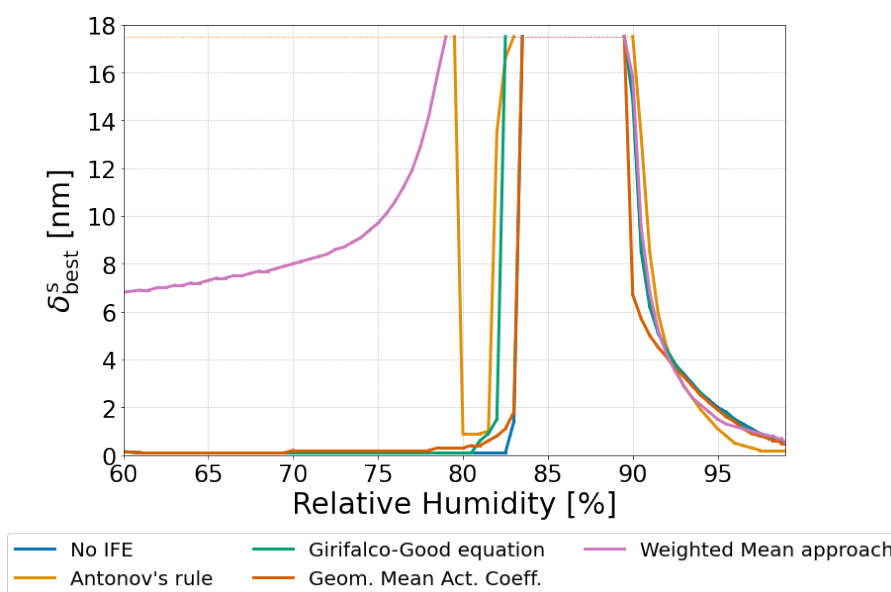
Figure 9. The δ^s value corresponding to the overall minimum in Gibbs energy of a 250 nm dry diameter particle for each interfacial tension treatment. The particle was composed of water, 1,2,6-hexanetriol, and ammonium sulfate with a 2:1 organic-to-inorganic dry mass ratio. δ^s values between 0.1–17.5 nm were tested.

Code and data availability. The experimental data and model outputs underlying all figures shown are provided in an electronic supplement. The size-dependent phase separation code is available upon request from the authors.

Author contributions. RS performed model development and simulations, visualized model outputs, and wrote the manuscript. AZ conceived the project, assisted with model development and theory, co-wrote the manuscript, was responsible for supervision, and secured funding for the work.

Competing interests. The authors have no competing interests to declare.

Financial support. This project was undertaken with financial support by the government of Canada through the federal Department of Environment and Climate Change (grant no. GCXE20S049) and the Natural Sciences and Engineering Research Council of Canada (NSERC grant no. RGPIN-2021-02688). RS was also supported by a doctoral scholarship from the Fonds de Recherche du Québec – Nature et technologies (FRQNT, scholarship no. 314186).

References

Amirfazli, A. and Neumann, A.: Status of the three-phase line tension: a review, Advances in Colloid and Interface Science, 110, 121–141, https://doi.org/https://doi.org/10.1016/j.cis.2004.05.001, 2004.

Antonov, G. N.: Sur la tension superficielle à la limite de deux couches, J. Chim. Phys., 5, 372–385, https://doi.org/10.1051/jcp/1907050372, 1907.

Aston, M. S. and Herrington, T. M.: The effect of added electrolyte on surface pressure/area per molecule isotherms, Journal of Colloid and Interface Science, 141, 50–59, 1991.

Aveyard, R. L. and Saleem, S. M.: Interfacial tensions at alkane-aqueous electrolyte interfaces, Journal of the Chemical Society, Faraday Transactions, 72, 1609–1617, https://doi.org/10.1039/F19767201609, 1976.

Bahramian, A.: Unlocking the Secrets of Liquid–Liquid Interfaces and Phase Equilibria: Exploring the Interplay of Critical Composition, Interfacial Tension, and Mutual Solubility, Langmuir, 40, 4684–4701, https://doi.org/10.1021/acs.langmuir.3c03344, pMID: 38381860, 2024.

Bahramian, A. and Danesh, A.: Prediction of liquid–liquid interfacial tension in multi-component systems, Fluid Phase Equilibria, 221, 197–205, https://doi.org/https://doi.org/10.1016/j.fluid.2004.04.012, 2004.

Bahramian, A. and Danesh, A.: Prediction of liquid–vapour surface tension in multi-component systems, Fluid Phase Equilibria, 236, 156–161, https://doi.org/https://doi.org/10.1016/j.fluid.2005.07.016, 2005.

Bertram, A. K., Martin, S. T., Hanna, S. J., Smith, M. L., Bodsworth, A., Chen, Q., Kuwata, M., Liu, A., You, Y., and Zorn, S. R.: Predicting the relative humidities of liquid-liquid phase separation, efflorescence, and deliquescence of mixed particles of ammonium sulfate, organic material, and water using the organic-to-sulfate mass ratio of the particle and the oxygen-to-carbon elemental ratio of the organic component, Atmospheric Chemistry and Physics, 11, 10 995–11 006, https://doi.org/10.5194/acp-11-10995-2011, 2011.

Binyaminov, H., Abdullah, F., Zargarzadeh, L., and Elliott, J. A. W.: Thermodynamic Investigation of Droplet–Droplet and Bubble–Droplet Equilibrium in an Immiscible Medium, The Journal of Physical Chemistry B, 125, 8636–8651, https://doi.org/10.1021/acs.jpcb.1c02877, pMID: 34310143, 2021.

Bzdek, B. R., Power, R. M., Simpson, S. H., Reid, J. P., and Royall, C. P.: Precise, contactless measurements of the surface tension of picolitre aerosol droplets, Chem. Sci., 7, 274–285, https://doi.org/10.1039/C5SC03184B, 2016.

Chan, M. N., Lee, A. K. Y., and Chan, C. K.: Responses of Ammonium Sulfate Particles Coated with Glutaric Acid to Cyclic Changes in Relative Humidity: Hygroscopicity and Raman Characterization, Environmental Science & Technology, 40, 6983–6989, https://doi.org/10.1021/es060928c, pMID: 17154005, 2006.

Ciobanu, V. G., Marcolli, C., Krieger, U. K., Weers, U., and Peter, T.: Liquidâˆ'Liquid Phase Separation in Mixed Organic/Inorganic Aerosol Particles, The Journal of Physical Chemistry A, 113, 10 966–10 978, https://doi.org/10.1021/jp905054d, pMID: 19775109, 2009.

Davies, J. F., Zuend, A., and Wilson, K. R.: Technical note: The role of evolving surface tension in the formation of cloud droplets, Atmos. Chem. Phys., 19, 2933–2946, https://doi.org/10.5194/acp-19-2933-2019, 2019.

Fowkes, F. M.: Determination of interfacial tensions, contact angles, and dispersion forces in surfaces by assuming additivity of intermolecular interactions in surfaces, The Journal of Physical Chemistry, 66, 382–382, https://doi.org/10.1021/j100808a524, 1962.

Fowkes, F. M.: Additivity of intermolecular forces at interfaces. I. determination of the contribution to surface and interfacial tensions of dispersion forces in various liquids, The Journal of Physical Chemistry, 67, 2538–2541, https://doi.org/10.1021/j100806a008, 1963.

Freedman, M. A.: Phase separation in organic aerosol, Chem. Soc. Rev., 46, 7694–7705, https://doi.org/10.1039/C6CS00783J, 2017.

Freedman, M. A.: Liquid–Liquid Phase Separation in Supermicrometer and Submicrometer Aerosol Particles, Accounts of Chemical Research, 53, 1102–1110, https://doi.org/10.1021/acs.accounts.0c00093, pMID: 32432453, 2020.

Gaston, C. J., Thornton, J. A., and Ng, N. L.: Reactive uptake of N_2O_5 to internally mixed inorganic and organic particles: the role of organic carbon oxidation state and inferred organic phase separations, Atmospheric Chemistry and Physics, 14, 5693–5707, https://doi.org/10.5194/acp-14-5693-2014, 2014.

Gervasi, N. R., Topping, D. O., and Zuend, A.: A predictive group-contribution model for the viscosity of aqueous organic aerosol, Atmospheric Chemistry and Physics, 20, 2987–3008, https://doi.org/10.5194/acp-20-2987-2020, 2020.

Girifalco, L. A. and Good, R. J.: A Theory for the Estimation of Surface and Interfacial Energies. I. Derivation and Application to Interfacial Tension, The Journal of Physical Chemistry, 61, 904–909, https://doi.org/10.1021/j150553a013, 1957.

Gorkowski, K., Donahue, N. M., and Sullivan, R. C.: Aerosol Optical Tweezers Constrain the Morphology Evolution of Liquid-Liquid Phase-Separated Atmospheric Particles, Chem, 6, 204–220, https://doi.org/https://doi.org/10.1016/j.chempr.2019.10.018, 2020.

Harkins, W. D. and Humphery, E. C.: The Surface-Tension at the Interface Between Two Liquids, Proceedings of the National Academy of Sciences, 1, 585–590, https://doi.org/10.1073/pnas.1.12.585, 1915.

Harris, M. T. and Byers, C. H.: An advanced technique for interfacial tension measurement in liquid- liquid systems, Tech. rep., https://doi.org/10.2172/5172058, 1989.

Hua, X., Bevan, M. A., and Frechette, J.: Reversible Partitioning of Nanoparticles at an Oil–Water Interface, Langmuir, 32, 11341–11352, https://doi.org/10.1021/acs.langmuir.6b02255, pMID: 27564252, 2016.

Huang, Y., Mahrt, F., Xu, S., Shiraiwa, M., Zuend, A., and Bertram, A. K.: Coexistence of three liquid phases in individual atmospheric aerosol particles, Proceedings of the National Academy of Sciences, 118, e2102512118, https://doi.org/10.1073/pnas.2102512118, 2021.

Intergovernmental Panel on Climate, C., ed.: Summary for Policymakers, pp. 1–30, Cambridge University Press, Cambridge, https://doi.org/DOI: 10.1017/CBO9781107415324.004, 2014.

Jimenez, J. L., Canagaratna, M. R., Donahue, N. M., Prevot, A. S. H., Zhang, Q., Kroll, J. H., DeCarlo, P. F., Allan, J. D., Coe, H., Ng, N. L., Aiken, A. C., Docherty, K. S., Ulbrich, I. M., Grieshop, A. P., Robinson, A. L., Duplissy, J., Smith, J. D., Wilson, K. R., Lanz, V. A., Hueglin, C., Sun, Y. L., Tian, J., Laaksonen, A., Raatikainen, T., Rautiainen, J., Vaattovaara, P., Ehn, M., Kulmala, M., Tomlinson, J. M., Collins, D. R., Cubison, M. J., null null, Dunlea, J., Huffman, J. A., Onasch, T. B., Alfarra, M. R., Williams, P. I., Bower, K., Kondo, Y., Schneider, J., Drewnick, F., Borrmann, S., Weimer, S., Demerjian, K., Salcedo, D., Cottrell, L., Griffin, R., Takami, A., Miyoshi, T., Hatakeyama, S., Shimono, A., Sun, J. Y., Zhang, Y. M., Dzepina, K., Kimmel, J. R., Sueper, D., Jayne, J. T., Herndon, S. C., Trimborn, A. M., Williams, L. R., Wood, E. C., Middlebrook, A. M., Kolb, C. E., Baltensperger, U., and Worsnop, D. R.: Evolution of Organic Aerosols in the Atmosphere, Science, 326, 1525–1529, https://doi.org/10.1126/science.1180353, 2009.

Kleinheins, J., Shardt, N., El Haber, M., Ferronato, C., Nozière, B., Peter, T., and Marcolli, C.: Surface tension models for binary aqueous solutions: a review and intercomparison, Phys. Chem. Chem. Phys., 25, 11055–11074, https://doi.org/10.1039/D3CP00322A, 2023.

Kucinski, T. M., Dawson, J. N., and Freedman, M. A.: Size-Dependent Liquid–Liquid Phase Separation in Atmospherically Relevant Complex Systems, The Journal of Physical Chemistry Letters, 10, 6915–6920, https://doi.org/10.1021/acs.jpclett.9b02532, pMID: 31638813, 2019.

Kwamena, Buajarern, J., and Reid, J. P.: Equilibrium Morphology of Mixed Organic/Inorganic/Aqueous Aerosol Droplets: Investigating the Effect of Relative Humidity and Surfactants, J. Phys. Chem. A, 114, 5787–5795, http://dx.doi.org/10.1021/jp1003648, 2010.

Lam, H. K., Xu, R., Choczynski, J., Davies, J. F., Ham, D., Song, M., Zuend, A., Li, W., Tse, Y.-L. S., and Chan, M. N.: Effects of liquid–liquid phase separation and relative humidity on the heterogeneous OH oxidation of inorganic–organic aerosols: insights from methylglutaric

acid and ammonium sulfate particles, Atmospheric Chemistry and Physics, 21, 2053–2066, https://doi.org/10.5194/acp-21-2053-2021, 2021.

Lang-Yona, N., Abo-Riziq, A., Erlick, C., Segre, E., Trainic, M., and Rudich, Y.: Interaction of internally mixed aerosols with light, Physical Chemistry Chemical Physics, 12, 21–31, https://doi.org/10.1039/B913176K, 2010.

640 Li, W., Teng, X., Chen, X., Liu, L., Xu, L., Zhang, J., Wang, Y., Zhang, Y., and Shi, Z.: Organic Coating Reduces Hygroscopic Growth of Phase-Separated Aerosol Particles, Environmental Science & Technology, 55, 16 339–16 346, https://doi.org/10.1021/acs.est.1c05901, pMID: 34894668, 2021.

Lilek, J. and Zuend, A.: A predictive viscosity model for aqueous electrolytes and mixed organic–inorganic aerosol phases, Atmospheric Chemistry and Physics, 22, 3203–3233, https://doi.org/10.5194/acp-22-3203-2022, 2022.

645 Makkonen, L. and Kurkela, J.: Another look at the interfacial interaction parameter, Journal of Colloid and Interface Science, 529, 243–246, https://doi.org/https://doi.org/10.1016/j.jcis.2018.06.015, 2018.

Malek, K., Gohil, K., Olonimoyo, E. A., Ferdousi-Rokib, N., Huang, Q., Pitta, K. R., Nandy, L., Voss, K. A., Raymond, T. M., Dutcher, D. D., Freedman, M. A., and Asa-Awuku, A.: Liquid–Liquid Phase Separation Can Drive Aerosol Droplet Growth in Supersaturated Regimes, ACS Environmental Au, 3, 348–360, https://doi.org/10.1021/acsenvironau.3c00015, 2023.

650 Marcolli, C. and Krieger, U. K.: Phase Changes during Hygroscopic Cycles of Mixed Organic/Inorganic Model Systems of Tropospheric Aerosols, The Journal of Physical Chemistry A, 110, 1881–1893, https://doi.org/10.1021/jp0556759, pMID: 16451021, 2006.

Ohno, P. E., Brandão, L., Rainone, E. M., Aruffo, E., Wang, J., Qin, Y., and Martin, S. T.: Size Dependence of Liquid–Liquid Phase Separation by in Situ Study of Flowing Submicron Aerosol Particles, The Journal of Physical Chemistry A, 127, 2967–2974, https://doi.org/10.1021/acs.jpca.2c08224, pMID: 36947002, 2023.

655 Ott, E.-J. E. and Freedman, M. A.: Inhibition of Phase Separation in Aerosolized Water-Soluble Polymer–Polymer Nanoparticles at Small Sizes and the Effects of Molecular Weight, The Journal of Physical Chemistry B, 124, 7518–7523, https://doi.org/10.1021/acs.jpcb.0c06535, pMID: 32790387, 2020.

Ott, E.-J. E. and Freedman, M. A.: Influence of Ions on the Size Dependent Morphology of Aerosol Particles, ACS Earth and Space Chemistry, 5, 2320–2328, https://doi.org/10.1021/acsearthspacechem.1c00210, 2021.

660 Ovadnevaite, J., Zuend, A., Laaksonen, A., Sanchez, K. J., Roberts, G., Ceburnis, D., Decesari, S., Rinaldi, M., Hodas, N., Facchini, M. C., Seinfeld, J. H., and O' Dowd, C.: Surface tension prevails over solute effect in organic-influenced cloud droplet activation, Nature, 546, 637–641, https://doi.org/10.1038/nature22806, 2017.

Paul, G. W. and De Chazal, L. M.: Interfacial tensions in ternary liquid-liquid systems, Journal of Chemical and Engineering Data, 12, 105–107, https://doi.org/10.1021/je60032a033, 1967.

665 Pliskin, I. and Treybal, R. E.: Interfacial Tensions in Two-Liquid-Phase Ternary Systems., Journal of Chemical and Engineering Data, 11, 49–52, https://doi.org/10.1021/je60028a013, 1966.

Rastak, N., Pajunoja, A., Acosta Navarro, J. C., Ma, J., Song, M., Partridge, D. G., Kirkevåg, A., Leong, Y., Hu, W. W., Taylor, N. F., Lambe, A., Cerully, K., Bougiatioti, A., Liu, P., Krejci, R., Petäjä, T., Percival, C., Davidovits, P., Worsnop, D. R., Ekman, A. M. L., Nenes, A., Martin, S., Jimenez, J. L., Collins, D. R., Topping, D., Bertram, A. K., Zuend, A., Virtanen, A., and Riipinen, I.: Microphysical

670 explanation of the RH-dependent water affinity of biogenic organic aerosol and its importance for climate, Geophysical Research Letters, 44, 5167–5177, https://doi.org/https://doi.org/10.1002/2017GL073056, 2017.

Reid, J. P., Dennis-Smither, B. J., Kwamena, N.-O. A., Miles, R. E. H., Hanford, K. L., and Homer, C. J.: The morphology of aerosol particles consisting of hydrophobic and hydrophilic phases: hydrocarbons, alcohols and fatty acids as the hydrophobic component, Phys. Chem. Chem. Phys., 13, 15 559–15 572, https://doi.org/10.1039/C1CP21510H, 2011.

675 Ruehl, C. R., Davies, J. F., and Wilson, K. R.: An interfacial mechanism for cloud droplet formation on organic aerosols, Science, 351, 1447–1450, https://doi.org/10.1126/science.aad4889, 2016.

Russell, L. M. and Ming, Y.: Deliquescence of small particles, The Journal of Chemical Physics, 116, 311–321, https://doi.org/10.1063/1.1420727, 2002.

Schmedding, R. and Zuend, A.: A thermodynamic framework for bulk–surface partitioning in finite-volume mixed organic–inorganic aerosol
680 particles and cloud droplets, EGUsphere, 2023, 1–42, https://doi.org/10.5194/egusphere-2023-336, 2023.

Schmedding, R., Rasool, Q. Z., Zhang, Y., Pye, H. O. T., Zhang, H., Chen, Y., Surratt, J. D., Lopez-Hilfiker, F. D., Thornton, J. A., Goldstein, A. H., and Vizuete, W.: Predicting secondary organic aerosol phase state and viscosity and its effect on multiphase chemistry in a regional-scale air quality model, Atmos. Chem. Phys., 20, 8201–8225, https://doi.org/10.5194/acp-20-8201-2020, 2020.

Shiraiwa, M., Zuend, A., Bertram, A. K., and Seinfeld, J. H.: Gas-particle particle partitioning of atmospheric aerosols: interplay of physical
685 state, non-ideal mixing and morphology, Phys. Chem. Chem. Phys., 15, 11 441–11 453, https://doi.org/10.1039/C3CP51595H, 2013.

Song, M., Marcolli, C., Krieger, U. K., Zuend, A., and Peter, T.: Liquid-liquid phase separation and morphology of internally mixed di-carboxylic acids/ammonium sulfate/water particles, Atmospheric Chemistry and Physics, 12, 2691–2712, https://doi.org/10.5194/acp-12-2691-2012, 2012.

Song, M., Marcolli, C., Krieger, U. K., Lienhard, D. M., and Peter, T.: Morphologies of mixed organic/inorganic/aqueous aerosol droplets,
690 Faraday Discuss., 165, 289–316, https://doi.org/10.1039/C3FD00049D, 2013.

Wang, P. and Anderko, A.: Modeling Interfacial Tension in Liquid–Liquid Systems Containing Electrolytes, Industrial & Engineering Chemistry Research, 52, 6822–6840, https://doi.org/10.1021/ie303460c, 2013.

Winter, A.: Antonow's rule 85 years later, Heterogeneous Chemistry Reviews, 2, 269–308, 1995.

Yin, H., Dou, J., Klein, L., Krieger, U. K., Bain, A., Wallace, B. J., Preston, T. C., and Zuend, A.: Extension of the AIOMFAC model
695 by iodine and carbonate species: applications for aerosol acidity and cloud droplet activation, Atmos. Chem. Phys., 22, 973–1013, https://doi.org/10.5194/acp-22-973-2022, aCP, 2022.

You, Y., Renbaum-Wolff, L., Carreras-Sospedra, M., Hanna, S. J., Hiranuma, N., Kamal, S., Smith, M. L., Zhang, X., Weber, R. J., Shilling, J. E., Dabdub, D., Martin, S. T., and Bertram, A. K.: Images reveal that atmospheric particles can undergo liquid–liquid phase separations, Proceedings of the National Academy of Sciences, 109, 13 188–13 193, https://doi.org/10.1073/pnas.1206414109, 2012.

700 You, Y., Smith, M. L., Song, M., Martin, S. T., and Bertram, A. K.: Liquid–liquid phase separation in atmospherically relevant particles consisting of organic species and inorganic salts, Int. Rev. Phys. Chem., 33, 43–77, https://doi.org/10.1080/0144235X.2014.890786, 2014.

Zhang, Q., Jimenez, J. L., Canagaratna, M. R., Allan, J. D., Coe, H., Ulbrich, I., Alfarra, M. R., Takami, A., Middlebrook, A. M., Sun, Y. L., Dzepina, K., Dunlea, E., Docherty, K., DeCarlo, P. F., Salcedo, D., Onasch, T., Jayne, J. T., Miyoshi, T., Shimono, A., Hatakeyama, S., Takegawa, N., Kondo, Y., Schneider, J., Drewnick, F., Borrmann, S., Weimer, S., Demerjian, K., Williams, P., Bower, K.,
705 Bahreini, R., Cottrell, L., Griffin, R. J., Rautiainen, J., Sun, J. Y., Zhang, Y. M., and Worsnop, D. R.: Ubiquity and dominance of oxygenated species in organic aerosols in anthropogenically-influenced Northern Hemisphere midlatitudes, Geophysical Research Letters, 34, https://doi.org/https://doi.org/10.1029/2007GL029979, 2007.

Zuend, A. and Seinfeld, J. H.: Modeling the gas-particle partitioning of secondary organic aerosol: the importance of liquid-liquid phase separation, Atmos. Chem. Phys., 12, 3857–3882, https://doi.org/10.5194/acp-12-3857-2012, 2012.

710 Zuend, A. and Seinfeld, J. H.: A practical method for the calculation of liquid–liquid equilibria in multicomponent organic–water–electrolyte systems using physicochemical constraints, Fluid Phase Equilibria, 337, 201–213, https://doi.org/10.1016/j.fluid.2012.09.034, 2013.

Zuend, A., Marcolli, C., Luo, B., and Peter, T.: A thermodynamic model of mixed organic–inorganic aerosols to predict activity coefficients, Atmospheric Chemistry and Physics, 8, 4559–4593, 2008.

Zuend, A., Marcolli, C., Peter, T., and Seinfeld, J. H.: Computation of liquid-liquid equilibria and phase stabilities: implications
715 for RH-dependent gas/particle partitioning of organic-inorganic aerosols, Atmospheric Chemistry and Physics, 10, 7795–7820, https://doi.org/10.5194/acp-10-7795-2010, 2010.

Zuend, A., Marcolli, C., Booth, A. M., Lienhard, D. M., Soonsin, V., Krieger, U. K., Topping, D. O., McFiggans, G., Peter, T., and Seinfeld, J. H.: New and extended parameterization of the thermodynamic model AIOMFAC: calculation of activity coefficients for organic-inorganic mixtures containing carboxyl, hydroxyl, carbonyl, ether, ester, alkenyl, alkyl, and aromatic functional groups, Atmospheric
720 Chemistry and Physics, 11, 9155–9206, https://doi.org/10.5194/acp-11-9155-2011, 2011.